Lithostratigraphy, lithofacies and deposition conditions of the late Olenekian-middle Anisian Alam Formation in the Nakhlak area, central Iran

Litoestratigrafía, litofacies y condiciones de depósito de la Formación Alam del Olekiniano tardío-Anisiano medio en el área de Nakhlak, Irán central

Payman **Rezaee**[1,*], Seyedeh Akram **Jooybari**[1], Kiamars **Hosseini**[1], Amin **Moodi**[1]

[1] Department of Geology, University of Hormozgan, Bandar Abbas, Iran.

* Corresponding author: (P. Rezaee)
p.rezaee@hormozgan.ac.ir

How to cite this article:
Rezaee, P., Jooybari, S.A., Hosseini, K., Moodi, A., 2023, Lithostratigraphy, lithofacies and deposition conditions of the late Olenekian-middle Anisian Alam Formation in the Nakhlak area, central Iran: Boletín de la Sociedad Geológica Mexicana, 75 (2), A070323. http://dx.doi.org/10.18268/BSGM2023v75n2a070323

Manuscript received: July 31, 2022.
Corrected manuscript received: January 2, 2023.
Manuscript accepted: March 5, 2023.

Peer Reviewing under the responsibility of Universidad Nacional Autónoma de México.

ABSTRACT

The present study aims to investigate petrography characteristics and sedimental environments of upper Olenekian–middle Anisian deposits of Nakhlak group in the sedimentary-structural zone of central Iran. To this end, a section of these deposits with a thickness of 720 meters was first selected, and 190 samples were taken from this section for preparing thin sections. Also, quantitative and qualitative laboratory tests were performed and 25 samples of sandstone were selected for point counter analysis. The results indicated that the major deposits of this formation are related to siliciclastic, carbonate, and pyroclastic types, which are in the form of two facies associations. The facies association A at the bottom of the studied section with the thickness of 90 meters has a periodicity of clastic, carbonate, and pyroclastic facies. The clastic facies of this association consists of fine-grained sandstone. In addition, the carbonate facies in association A are characterized by two microfacies consisting of intraclast oolitic grainstone and oolitic grainstone. Further, tuffite is the only pyroclastic facies related to association A, which has a laminate structure, cross-bedding lamination, herringbone bedding, and upward-thinning and thickening cycles. The facies association, B which is deposited later, is more in the middle and top part of the section. The facies association B is 660 meters thick and has a periodicity of clastic and limestone facies. Clastic facies of this association includes four lithofacies such as conglomerate, pebble coarse-grained sandstone, medium-grained sandstone to thin layer siltstone and shale. The carbonate facies consists of four microfacies such as sandy intraclastic wackestone and mudstone. Furthermore, slumping structures, cross bedding, turbulence, boudinage structure, and convolute of sediments, along with the effects of erosional channels are observed in facies B. Field and laboratory studies conducted on this succession indicate the structure of facies association A was deposited in a mixed siliciclastic carbonate ramp. Finally, submarine canyons and submarine fan environments were left by increasing the depth of the facies association B in the deep part of sea and turbidity systems.

Keywords: petrography, depositional environments, Upper Olenekian-Anisian, Alam Formation.

RESUMEN

El objetivo del presente estudio está dirigido a la investigación de las características petrográficas y los ambientes sedimentarios de los depósitos antiguos de los Olenekianos Anisianos Medio, hecho por el grupo Nakhlak, en la zona sedimentaria-estructural del centro de Irán. Con este fin, se seleccionó una parte de estos depósitos con un espesor de 720 metros y después se tomaron 190 muestras de esta parte para preparar secciones finas. También, se realizaron pruebas de laboratorio cuantitativas y cualitativas y se seleccionaron 25 muestras de arenisca para el análisis de contadores de puntos. Los resultados indicaron que los principales depósitos de esta formación están relacionados con tipos siliciclásticos, carbonatados y piroclásticos, que son en forma de dos asociaciones facies. La asociación de facies de "A" al principio de la parte estudiada con el espesor de 90 metros, tiene una periodicidad de facies clásicas, carbonatadas y piroclásticas. Las facies clásicas de esta asociación consisten en arenisca de grano fino. Además, las facies carbonatadas en la asociación "A" se caracterizan por dos micro facies que consisten en piedra granulada intra oolítica y piedra granulada oolítica. Además, la toba es la única facies piroclásticas relacionadas con la asociación "A", que tiene una estructura laminada, laminación cruzada, lecho de espiga y ciclos de adelgazamiento y engrosamiento ascendentes. La asociación de facies "B", que se deposita más tarde, se observa más en la parte media y final de la sección examinada por este estudio. La asociación facies de "B" es de 660 metros de largo y tiene una periodicidad de facies clásicas y calizas. Las facies clásicas de esta asociación incluyen cuatro litófagas tales como conglomerado, piedra arenisca de grano grueso, arenisca de grano medio a fina capa de limolita y esquisto. Las facies de carbonato se componen de cuatro micro facies como wackestone, intraclástico, arenoso y mudstone. Además, en la facies "B" se observaron estructuras empinadas, lecho cruzado, turbulencia, estructura de boudinage y complejidad de los sedimentos junto con los efectos de los canales de erosión. Los estudios de campo y de laboratorio realizados sobre esta sucesión indicaron la estructura del depósito de asociación de facies "A" en una rampa de carbonato siliciclástico mixto. Por último, los cañones submarinos y los entornos de los ventiladores submarinos se dejan al aumentar la profundidad de la asociación facies B en la parte profunda del mar y los sistemas de turbidez.

Palabras clave: petrografía, ambientes deposicionales, Olenekianos-Anisianos superior, Formación de Alam.

http://dx.doi.org/10.18268/BSGM2023v75n2a070323

1. Introduction

The study of lithofacies is of great importance, especially in clastic sediments since the lithofacies are deposited in special environments under certain sedimentary processes (Rossi *et al.*, 2017; Hopkins *et al.*, 2020). Thus, recognizing lithofacies plays an important role in interpreting the processes concurrent with sedimentation. Moreover, identifying facies can significantly contribute to the reconstitution of the sedimentary environment and depositional conditions (Miall, 2000; Catuneanu, 2022; Rezaee *et al.*, 2022). The composition of clastic rocks is affected by factors such as tectonic activity, source rock characteristics, degree of weathering, and transportation (Garzanti, 2019; Martizzi *et al.*, 2021; Nikbakht *et al.*, 2022). The Triassic sedimentary succession (Nakhlak group) located in the northeast of Anarak town in Central Iran is significantly different from its equivalent sedimentary succession in Iran. In addition, Triassic sedimentary succession is similar to those of the Aqdarband group in northeastern Iran (Davoudzadeh and Seyed-Emami, 1972; Alavi *et al.*, 1997; Vaziri, 2001) (Figure 1). These sequences are similar to the sequence of sediments in northern Afghanistan and were deposited in an epicontinental sea (Ghorbani, 2019). The present study aims to evaluate the lithofacies and deposition conditions of late Olenekian to middle Anisian deposits in the Nakhlak group (Alam Formation) regarding the field and laboratory characteristics. The present study can make a significant contribution to understanding the history of Alam deposition in the Central Iran basin during the Triassic.

2. Geological setting

The area under study is the Nakhlak group located in the Central Iran zone, 60 km away from Anarak (Figure 1).

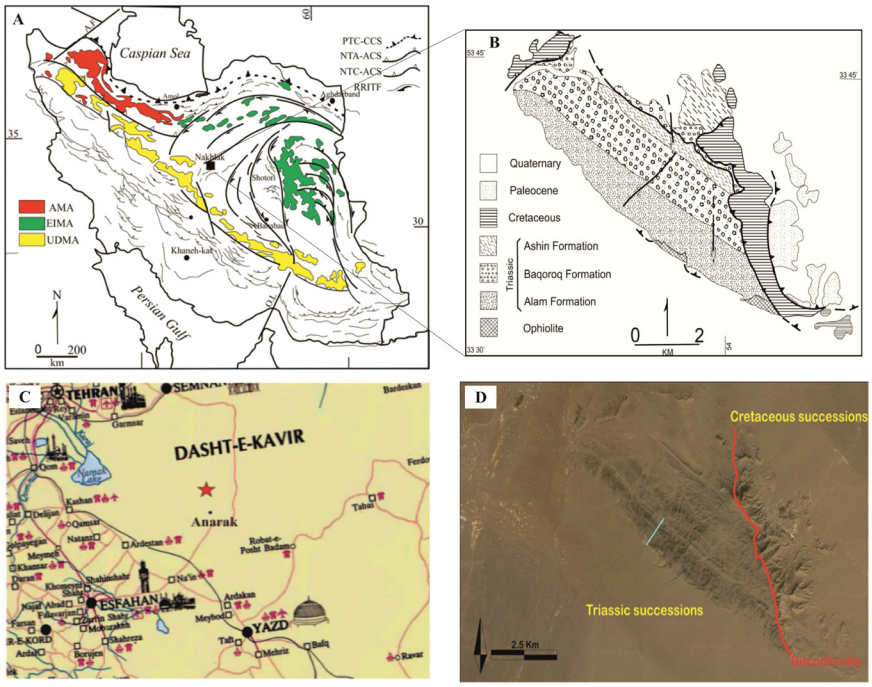

Figure 1 A: Map of structural components of Iran and related faults: (Alavi, 1991). (AMA: Alborz Magmatism Collection. EIMA: Eastern Iran Magmatism Collection. UDMA: Urmia-Daghter metamorphic complex. PCC-CCS: Paleotethys continent-continent collision. NTA-ACS: Neotethys collisional joint. PRITF: strike-slip faults associated with intracontinental rotations. O.L: Oman line) B: Geological map of Nakhlek group C: Map of access roads to Nakhlak group and Alam Formation D: The direction of the transect is located in the Nakhlak group in the satellite maps.

http://dx.doi.org/10.18268/BSGM2023v75n2a070323

The Nakhlak group is considered one of the most challenging stratigraphic and tectonic zones in Central Iran (Davuodzadeh and Seyed-Emami, 1972; Ruttner, 1993; Syed-Emami, 2003; Balini *et al.*, 2009). This group consists of Alam, Baqoroq, and Ashin formations (Davoudzadeh and Seyed-Emami, 1972; Alavi *et al.*, 1997; Vaziri, 2001; Balini *et al.*, 2009) (Figure 2). The sequences of upper Olenekian–middle Anisian (Alam formation) are regarded as the oldest deposits in the Nakhlak group in the sedimentary-structural zone of Central Iran, and the age of these deposits is specified by the presence of ammonites and bivalves (Tozer, 1972; Vaziri, 2001; Vaziri and Fursich, 2007; Balini *et al.*, 2009).

This sequence includes sandstone and shale layers, which are interlayered and generally have volcanic debris (Hashemi Azizi *et al.*, 2018). The rocks in the active continental margin environment of the Triassic Nakhlak group are significantly different from the other equivalent carbonate platform sediments (Elika and Shotori formations) deposited in many regions in Iran (Alavi *et al.*, 1997; Seyed-Emami, 2003; Balini *et al.*, 2009) and have platform conditions near the continent (Şengör, 1979; Stampfli *et al.*, 1991; Dercourt *et al.*, 2000; Stampfli and Borel, 2002; Brunet *et al.*, 2003; Torsvik and Cocks, 2004; Angiolini *et al.*, 2007). In the Early Triassic Period, the marine sedimentary conditions were confirmed in a forearc position in the active margins of south Eurasia by the siliciclastic-carbonate sequence of the Alam Formation, which generally included volcanic clastic rocks related to the arc activity (Hashemi Azizi *et al.*, 2018). Then, this basin was filled with sediments in the Anisian stage and the conditions changed from marine to continental, and, consequently, the conglomerate Baqoroq formation was deposited

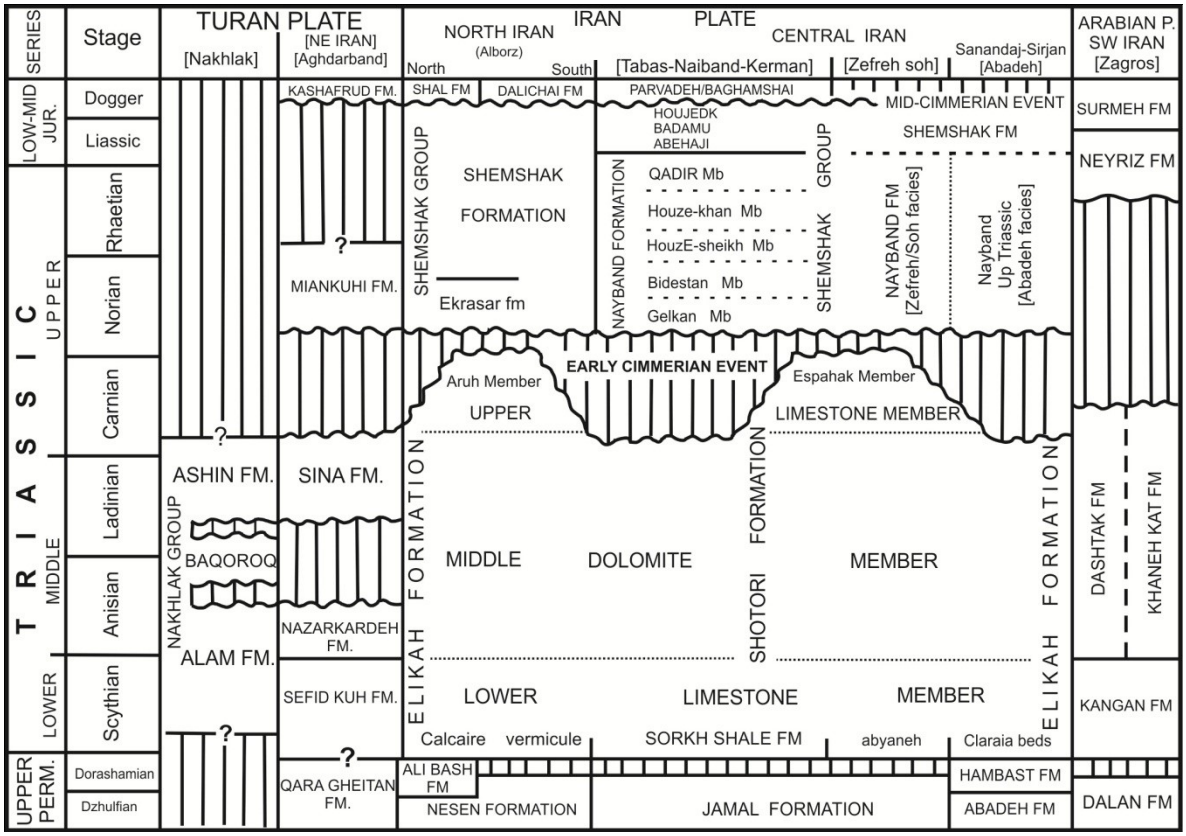

Figure 2 Stratigraphic columns of the Triassic formations in Iran (Ghorbani, 2019).

http://dx.doi.org/10.18268/BSGM2023v75n2a070323

Table 1. Counted parameters for point-counter analysis.

Counted Parameters	Recalculated Parameters
Qm non=Non-undulose Monocrystaline quartz	Q=Qm+Qpq (Folk,1974 classification)
Qm un= Undulose Monocrystalline quartz	Qp=Qpq+Cht
Qpq=Polycrystalline quartz	Qt= Qm+Qp
Qpq 2-3=Qp 2-3 crystal units per grain	F=P+K
Qpq>3=Qp>3 crystal units per grain	L=Lv+Ls+Lsm
Cht=Chert	Qm=Qm non+Qm un
P= Plagioclase feldspar	Lt=L+Qp
K=Potassium feldspar	RF=L+Cht (Folk,1974 classification)
Ls= Sedimentary lithics	Acc=Accessory minerals
Lsm=Metasedimentary lithics	Cem=Cements
Lv=Volcanic hypabyssal lithics	M=Matrix
Lc=Carbonate rock fragment	Lvm=Lv+xLm
	Lsm=Ls+(1-x)Lm
	x=Fraction of metavolcanics in Lm (Ingersoll and Suczek,1979)
	Acc=Accessory minerals

(Hashemi Azizi *et al*., 2018). The direction of the transect is located in the Nakhlak group in the Ghaleh Bozorg mountain with NW–SE direction in Yazd block, Central Iran (Figure1D).

3. Methods

The thickness of the layers was measured using a tape measure, compass, and Jacob's bars, along with two reciprocating modification phases using the method of Ceo (2010). In addition, sedimentary structures, lithofacies, and environmental evidence were recorded in macro dimensions, as well as palaeodip and sedimentary structures, including faults and slumping structures. The selected sample consisted of 190 thin sections to create thin sections and qualitative and quantitative laboratory analyses have been carried out on them. Twenty-five samples of sandstones were selected for point-counter analysis, and about 300 points were counted in each thin section by the method of Dickenson (1988) (Table 2) using the parameters defined in Table 1. Qualitative analyses were performed by identifying lithofacies and biofacies, evaluating environmental evidence, and determining the components of the facies. Furthermore, clastic and pyroclastic facies were named using the methods of Folk (1974) and Pettijohn *et al*. (1987) respectively. Moreover, carbonate facies were categorized by adopting the classification methods as proposed by Dunham (1962). They were, then, compared with the standard facies suggested by Flugel (2010) and Wilson (1975).

4. Discussion

4.1. LITHOSTRATIGRAPHY

Alam Formation deposits are underlain by the Neoproterozoic metamorphic units with a thrust fault boundary (Almasian, 1997) and are covered by the Baqoroq Formation with an erosional boundary (Figure 3). Due to the differences in the lithostratigraphy, the Alam Formation is divided into 23 units (Figure 4). The section of these deposits is 720 m thick with mainly siliciclastic and carbonate sediments, as well as the interlayers of pyroclastic sediments, which are presented on the stratigraphic column in Figure 5 and Table 3.

4.2. LITHOFACIES

Facies associations including A(shallow facies) and B (deep facies) were identified in the sequence of upper Olenekian–middle Anisian deposits (Alam Formation).

http://dx.doi.org/10.18268/BSGM2023v75n2a070323

Table 2. Results of point-counter analysis of 25 samples of sandstone from the Alam Formation. Abbreviations defined in Table 1.

S.N	Qm non	Qm un	Qpq 2-3	Qpq >3	K	P	Lv	Ls	Lsm	Lc	Cht	Acc	Sum	QM	Qp	Qt	F	L	Lt	RF
1	46	63	13	12	140	0	10	9	0	2	3	2	300	109	28	137	140	21	49	24
2	26	25	17	15	178	7	11	1	0	3	15	2	300	51	47	98	185	15	62	30
3	56	38	32	41	19	0	30	0	0	48	36	0	300	94	109	203	19	78	187	114
4	60	27	36	30	15	0	41	0	0	44	45	2	300	87	111	198	15	85	196	130
5	56	50	18	25	19	6	49	3	0	53	20	1	300	106	63	169	25	105	168	125
6	56	44	24	60	16	0	19	0	0	34	47	0	300	100	131	231	16	53	184	100
7	67	29	28	34	26	0	36	0	0	48	32	0	300	96	94	190	26	84	178	116
8	45	25	15	20	133	5	30	5	0	0	19	3	300	70	54	124	138	35	89	54
9	49	19	9	20	147	4	9		0	9	34	0	300	68	63	131	151	18	81	52
10	64	18	19	38	119	4	5	3	0	15	15	0	300	82	72	154	123	23	95	38
11	69	21	18	29	110	1	16	0	0	15	19	2	300	90	66	156	111	31	97	50
12	49	11	14	22	120	4	15	5	0	32	26	2	300	60	62	122	124	52	114	78
13	44	23	19	32	122	6	15	5	0	2	30	2	300	67	81	148	128	22	103	52
14	42	58	40	39	65	15	17	0	3	0	19	2	300	110	98	208	80	20	118	39
15	102	121	2	14	39	10	1	0	0	2	7	2	300	223	23	246	49	3	26	10
16	60	49	9	22	28	0	59	19	3	18	28	5	300	109	59	168	28	99	158	127
17	59	36	39	50	16	0	30	0	0	30	40	0	300	95	129	224	16	60	189	100
18	45	33	29	34	15	9	60	0	0	36	39	0	300	78	102	180	24	96	198	135
19	71	30	24	21	21	1	49	0	0	21	62	0	300	101	107	208	22	70	177	132
20	75	30	36	38	22	0	45	0	0	19	35	0	300	105	109	214	22	64	173	99
21	118	33	28	39	55	3	5	0	0	7	12	0	300	151	79	230	58	12	91	24
22	50	59	15	30	23	0	53	0	0	56	14	0	300	109	59	168	23	109	168	123
23	70	44	32	29	69	2	0	0	0	23	31	0	300	114	92	206	71	23	115	54
24	67	59	4	19	25	1	67	0	0	9	49	0	300	126	72	198	26	76	148	125
25	51	69	10	20	115	4	13	3	0	0	15	0	300	120	45	165	119	16	61	31

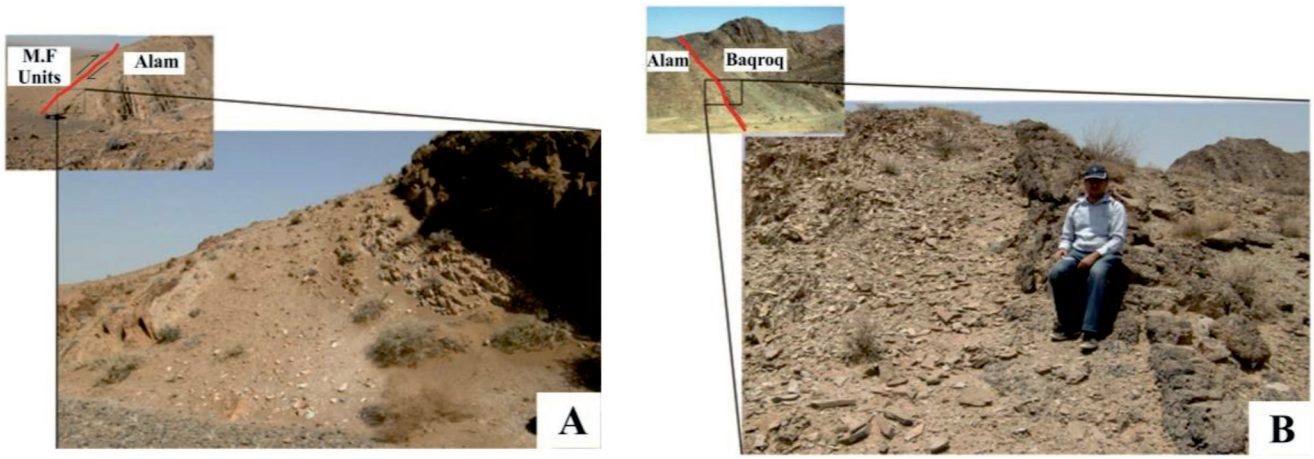

Figure 3 (A) The lower fault boundary of the Alam formation with metamorphic units (M.F) attributed to the Neoproterozoic. (B) The upper erosion boundary of the Alam formation with the Baqoroq formation.

http://dx.doi.org/10.18268/BSGM2023v75n2a070323

Table 3. Description of the identified units in Uupper Olenekian--Anisian deposits (Alam Formation).

Unit	Description	thickness (m)
1	Dolomitic limestone, brown to cream color, with deformation and banding folded face.	6
2	Dolomitized gray limestone, thinning-upward. orange to very light brown color.	10
3	Tuffite, bright green to white color mixed with lime, thinning upward.	9
4	Gray limestone with secondary calcitic veins, which gradually turns into a mixture of tuffite and limestone microlayer at the top.	5
5	Massive gray limestone with secondary white calcitic veins that turns into a nodular form at the top of the layer with tuffite interlayers. This subdivision involves two thickening-upward cycles including cross lamination.	13
6	Gray limestone with secondary calcitic fractures, milky in color, and changes gradually from sandstone units at the bottom of the layer to limestone at the top. The upper boundary of the layer is a limestone–sandstone boundary.	7
7	Calcareous sandstone with dolomitized lamination and secondary veins together with concentration of dolomitic layers. Narrow horizons contain fine-grained conglomerate lenses with diameters of 30 to 40 cm and thicknesses of 1 cm.	4
8	Massive gray limestone with individual horizons containing carried lime with lenses with cross lamination. The thickness of these lenses ranges 30-50 cm, and their diameter is about 2-3 m. Sandstones with cross-layering occur in the entire unit.	17
9	Limestone and tuffite have lamination fabric, shaly limestone with cross lamination fabric, together with sandstone with many existing erosional channels at the top.	29
10	Carried limestone frequentation together with shaly sandstone, amethyst color, sandstone-conglomerate frequentation with particle size of 3 to 5 mm in the form of long lenses.	34
11	Sandstone is available with layers of lime mud, clay, silt, and red to brown with the thickness of 2-3 cm and a lateral expansion of about 10m. The sand-shale cycle is repeated with clay and silt horizons. The sandstones are green at the weathered surface.	11
12	Thin-layer and thick-layer bioclastic lime	1
13	Medium-layer sandstone with tuffite horizon and shaly lamination fabric with a diameter of 30 cm	13
14	Tuffite	1
15	Two-meter sandstone with lamination fabric at the bottom, coarse-grained with the size of fine-grained conglomerate, together with cavitation erosion and cross-layering.	9
16	Light-green tuffite	1
17	Layered sandstone, thinning-upward, in addition to numerous coarse-grained layers with a thickness of 40-50 mm and cavitation erosion	7
18	Sandstone-shale-sandstone frequentation with cross-lamination and lamination besides sandstone-shale horizons with a light color in the middle part	30
19	Sandstone, black on weathered surfaces and graphite gray on fresh surfaces.	3
20	Thirteen meter coarse-grained sand–shale fining upward to fine-grained sand-shale, along with cycles of coarse-grained sand-shale (a cycle defect is seen between the two sandstone layers). Sandstone coarsening upwards, ended in gray and green shales.	75
21	Shale, amethyst in color, in the form of large layers of shale or shaly sand cycles, each cycle ending with 10 cm sand. There is more of the shale and less of the sandstone from the bottom to the top.	48
22	Lime mud-mudstone and amethyst sandstone frequentation. Lime mud-mudstone has slumping structures at the top and 1 cm sandy interlayer with lamination fabric, cross-lamination, and tangled classification. Cavitation erosion and 25 cm clasts, 10 cm lime fragments, and a coarse-grained conglomerate horizon at the top. There is a sandstone interlayer in the form of long and frequent lenses.	179
23	Nodular gray limestone, sandy limestone, and lime sandstone with 3-4 cm lime clasts. Lime sandstone has lamination and nodular gray limestone medium-layer with secondary calcite vein at the top of a thick layer of shaly lime.	212

http://dx.doi.org/10.18268/BSGM2023v75n2a070323

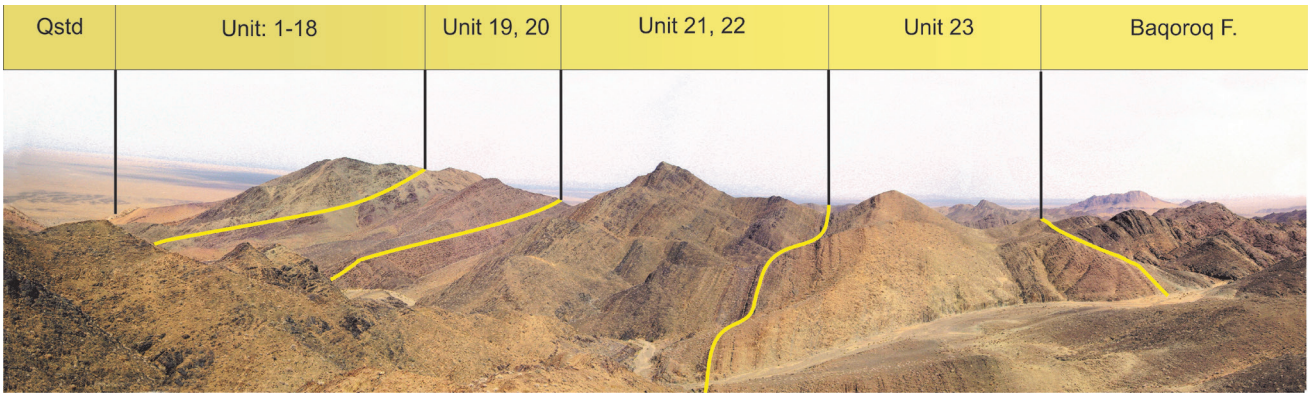

Figure 4 Identified units in Upper Olenekian–Anisian deposits (Alam Formation) looking west.

4.2.1. Facies association A

Facies association A is 90 m thick (Units 1-10) and includes a sequence of carbonate-clastic and pyroclastic facies. The structures on this association include stratification structures, and cross-bedding and herringbone cross-bedding stratification with thinning- and thickening-upward cycles. The following section describes the macroscopic and microscopic characteristics related to these facies.

4.2.1.1. Carbonate facies

These facies are orange to light brown and less gray in the desert. All the units are more or less dolomitized. In addition, these facies are like gathered dolomites in fractures. They have sedimentary lamination and cross bedding lamination structures. The intermittent presence of sand and sand load is observed in these units (Figure 6). The characteristics of these microfacies are as follows.

Petrography

MF1: Oolitic Grainstone: This facies of the gray limestone is carried with secondary calcite fracture and enclosed between two layers of limestone (Unit 5 and 6). The fabric of this microfacies is grain-supported and lacks mud. Ooid grains are the most frequent allochems, while intraclasts are rarely found.

Ooids are replaced by pyroclastic tuff. (Figure 7A). The size of the ooids is between 0.5 and 1 mm and they are in spherical, elliptical, and elongated shapes.

MF2: intraclast oolitic packstone/grainstone: This microfacies is carried lime and with lamination. The fabric is grain-supported and the mud content is low. The most abundant allochem is ooid, and then intraclast replaced by calcite. In addition, quartz and feldspar grains have sizes ranging from silt to 1 mm (<5%). Ooid grains range in size from 0.5 to 1 mm and are often spherical in shape. Intraclast particle sizes range from 1.5 to 2.5 mm and are often elongated. (Figure 7B).

Interpretation: The low mud content of these microfacies, along with the presence of ooid and intraclast, indicate high energy environmental conditions (Mass *et al.*, 2003; Flugel, 2010). These carbonate facies, due to the presence of sorting grains along with low mud content and the presence of ooids, indicate the sand shoal margin of the shelf (Fiugel, 2010). This microfacies can be equivalent to the standard facies SMF15 of Wilson (1975) and belongs to the facies zone as fZ6 (Wilson, 1975; Flugel, 2010).

4.2.1.2. Pyroclastic facies

Pyroclastic facies are seen as carried calcareous clasts with light green to white color. This facies has lamination and transport evidence (Figure 8A).

Petrography

P1: Tuffite: This pyroclastic facies has transported bright green to white lime particles. There are also laminae with carriage evidence. Fractures

http://dx.doi.org/10.18268/BSGM2023v75n2a070323

are dolomitized and these dolomites are euhedral. Tuffite facies have about 5% unrounded quartz of 0.1 mm, as well as the presence of feldspar crystals at the beginning of formation. The quartz amount increases upward to about 10% with a grain size of 0.2 mm (Figure 8B). *Interpretation:* This facies is the result of volcanic material entering the shallow sedimentary basin (Tucker, 2001).

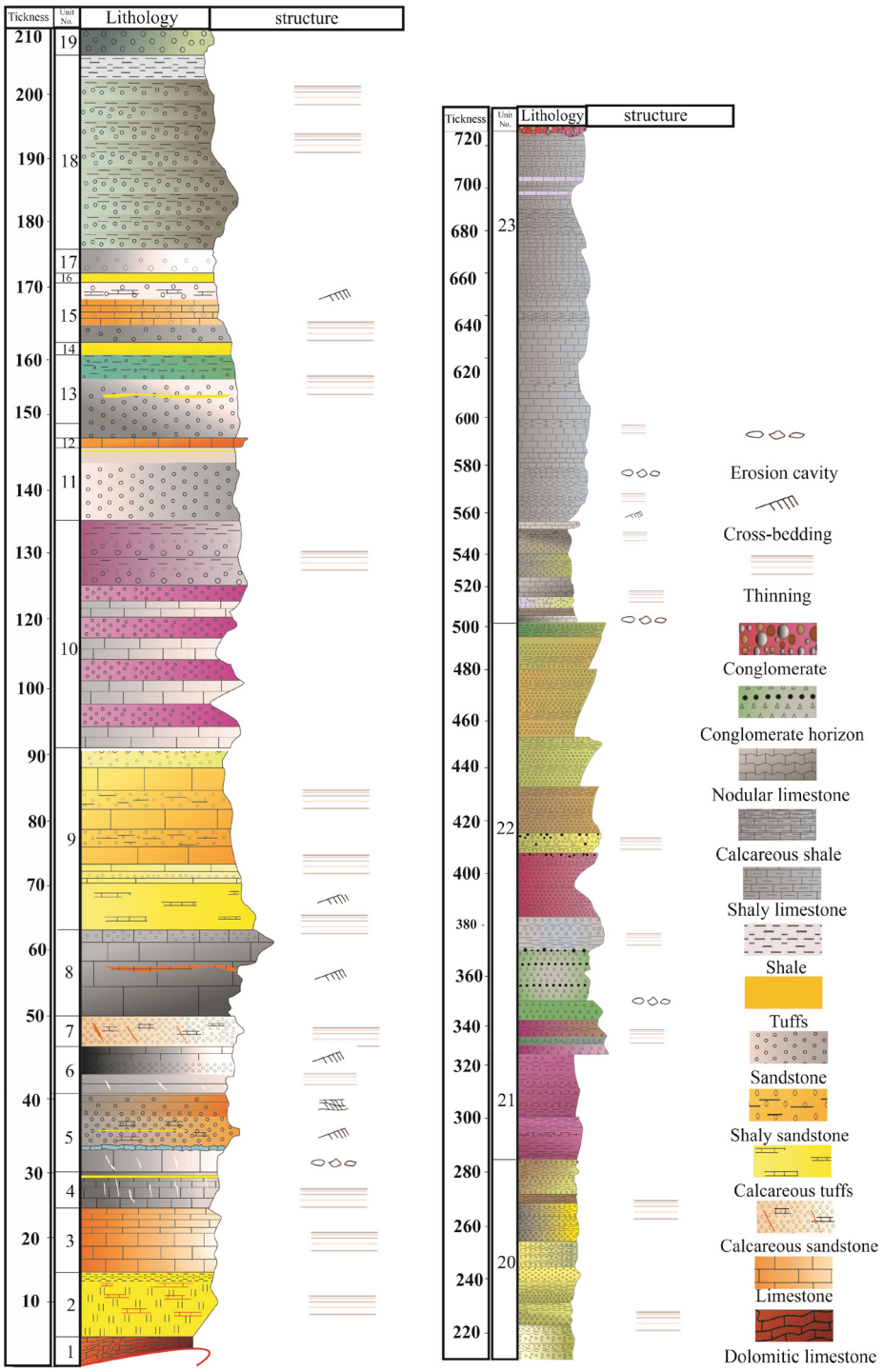

Figure 5 Lithostratigraphic column and petrofacies in uper Olenekian-Anisian deposits (Alam Formation).

http://dx.doi.org/10.18268/BSGM2023v75n2a070323

4.2.1.3. Clastic facies

L1: Fine-grained sandstone facies: The sandstones are fine-grained at the bottom of the section and have few fossil remnants. They are intermittent with shale and lime layers. They have fractures that have been filled by lime and are light brown to dark orange. In these facies, laminated, cross-bedding laminated structures, herringbone cross stratification, upward-thinning, and top-thinning structures are observed. Moreover, in terms of texture, they have medium and semi-angular sorting (Figure 9). *Interpretation:* The presence of these sedimentary structures, along with the intermittence of sandstone with limestone layers, indicates that the facies were deposited in a mixed siliciclastic carbonate ramp (Tucker and Wright, 1990).

Petrography clastic facies

The results of point counting and drawing data on the Folk triangle (Folk, 1980) show that the types of these sandstones are Arkose and Litharnite (Figure 10).

PF1:Arkose sandstone: This sandstone has a light brown color and is mainly in sequence with destructive limestone (Units 1,3,9). The quartz content of this petrofacies is between 33% and 46% and the feldspar is between 47% and 62%. In addition, the amount of lithic fragments is between 5% and 7% and feldspar grains are mainly semi-rounded and sericitized.

In general, plagioclase and alkali feldspars are indistinguishable. The quartz has angular to low-rounded particles with medium to poor sorting, and the average size of the grains is 0.15–0.2 mm. These petrofacies have fractures and veins which are sometimes filled with silica and sometimes seen as channel porosity (Figure 11A). Some of these lithic fragments are lime and dolomitized.

PF2: Litharenite sandstone: The Litharenite sandstone is a light-brown to dark-orange color,

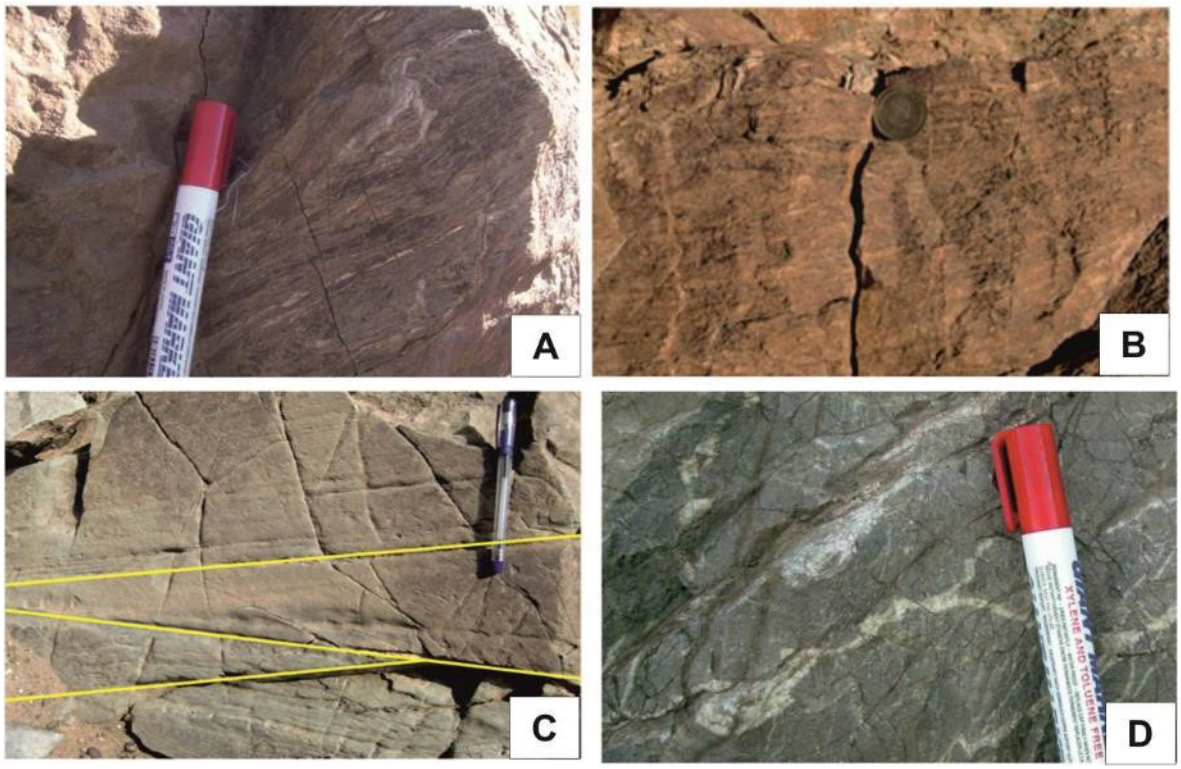

Figure 6 (A) and (B) Limestone units with lithoclast and schistosity from tectonic movements at the bottom of the section. (C) Herringbone bedding in calcareous units carried at the bottom of the section. (D) Lithodemic gray limestone with secondary fractures.

http://dx.doi.org/10.18268/BSGM2023v75n2a070323

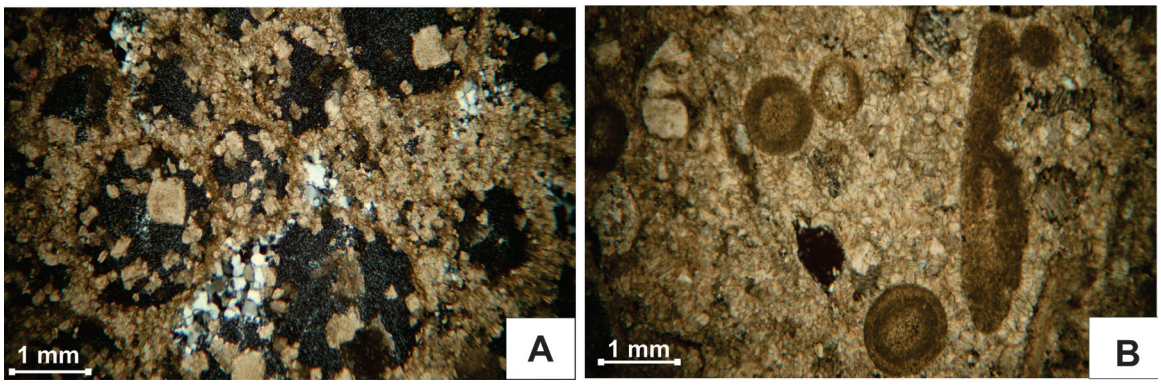

Figure 7 Photomicrographs using crossed polars. (A) MF1: Oolitic grainstone. (B) MF2: Intraclast oolitic packstone/grainstone.

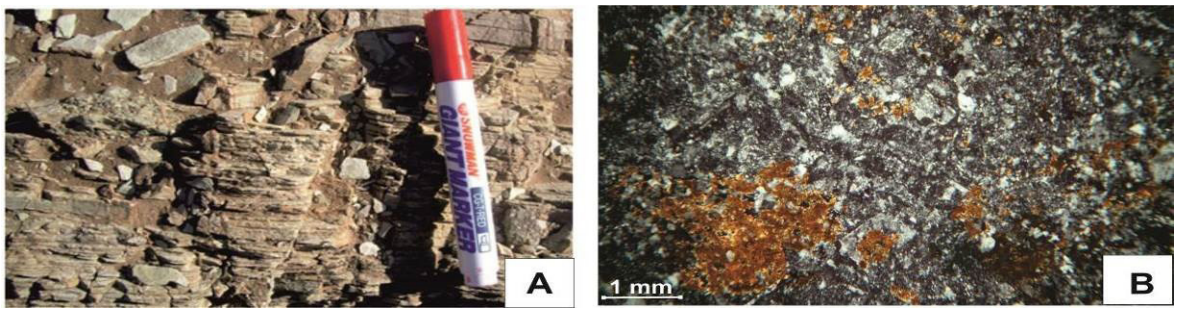

Figure 8 (A) Tuff-tuff has lamination (layering in a pyroclastic sequence). (B) Photomicrograph using crossed polars. P1: Tuffite.

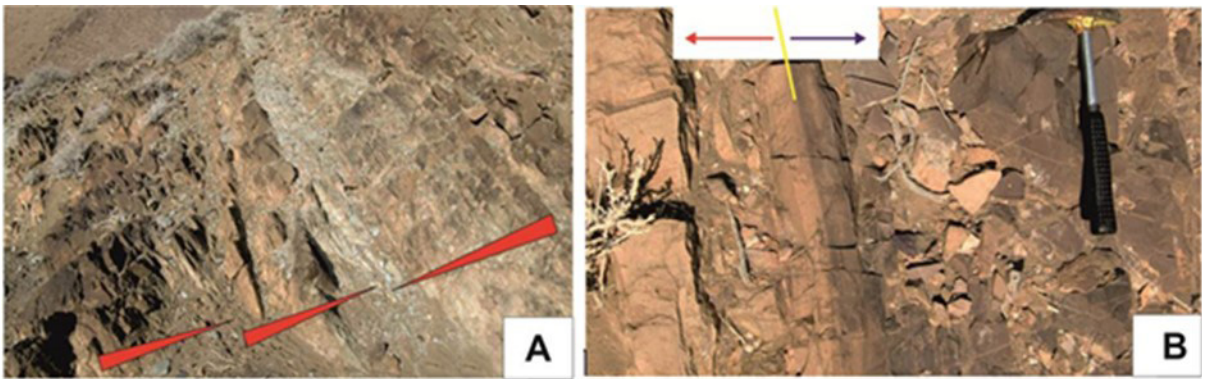

Figure 9 (A) Alternating calcareous sandstone-limestone-tuffite. The top of the red triangles indicate the thinning of the layers above. (B) The boundary between the change in color and the appearance of the facies and the emergence of shale-sandstone units. Red arrow: destroyed calcareous sandstone in orange. Blue arrow: calcareous sandstone and starting intermediate shale-sandstone-tuff units.

http://dx.doi.org/10.18268/BSGM2023v75n2a070323

along with lamination, and fractures are filled with dolomite (Unit 7). The quartz content of this petrofacies is between 56% and 77%, the feldspar is between 5% and 9%, and the amount of lithic fragments is between 17% and 35%. In general, clastic grains are mostly quartz, fine- to medium-grained, sub-angular, and with medium sorting.

High corrosion is obvious in some of the clastic grains, which are surrounded by lime in the form of cement. The calcareous lithic fragment in Figure 11B is a calcarenite based on Folk (1980).

4.2.2. Facies association B

Facies association B are 660 m thick. Existing facies are intermittent with of clastic-carbonated facies. In facies association B, there are structures including slumping, boudinage, cross-bedding classification, turbulence and tangle in sediments, and the remnants of erosional channel, which are described below as microscopic.

4.2.2.1. Carbonate facies

The sediments in this facies are mostly gray. These sediments originate from the destruction of sediments in shallow areas of the sea and are transported to a deep environment and deposited on the continental slope. They are seen in a rhythmic state with shale, and due to their deposition on the continental slope, boudinage structure is created in them. These limestones are seen with sandstones at the end of the section and possess Ammonoid macrofossils (Figure12).

Petrography

MF3: Sandy intraclast wackestone/packstone: They are found as limes with secondary calcite veins, which are layered in the upper parts of the unit with lamination (Units 15,17,20, 22). The fabric of this microfacies is mud-support to grain-supported. Intraclasts can be observed with the medium size of 1.5 mm and in irregular to elongated shapes. Intraclasts are often micriticized. There are traces of bioclasts found in this microfacies intraclast wackestone like the remains of bivalves. The quartz content of this microfacies is more than 5%, as scattered fine grains. (Figure 13A).

MF4: mudstone: Mudstones are dark layers with lamination and cross-bedding lamination. A large amount of degenerated limes and tuffites are found within shale layers in interbedded with

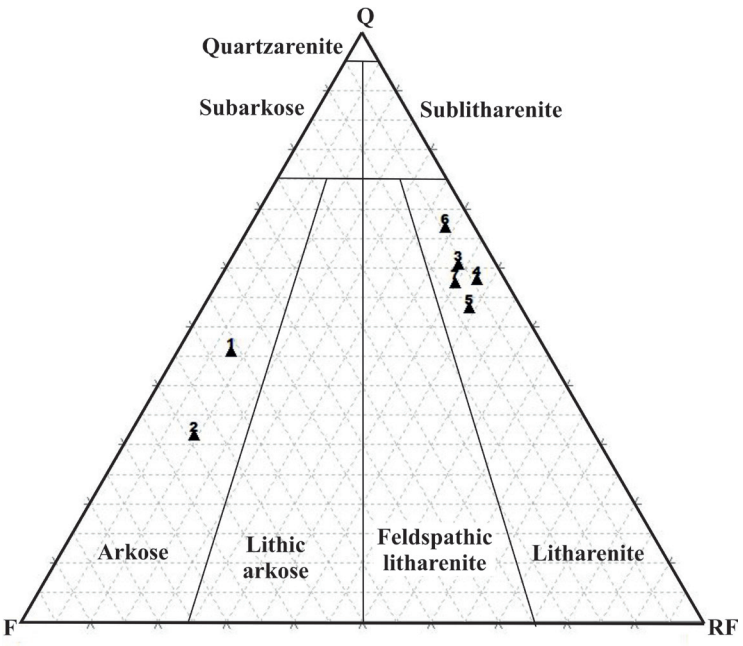

Figure 10 Data of facies association A on the sandstone classification on a QFR diagram(Folk, 1980).

http://dx.doi.org/10.18268/BSGM2023v75n2a070323

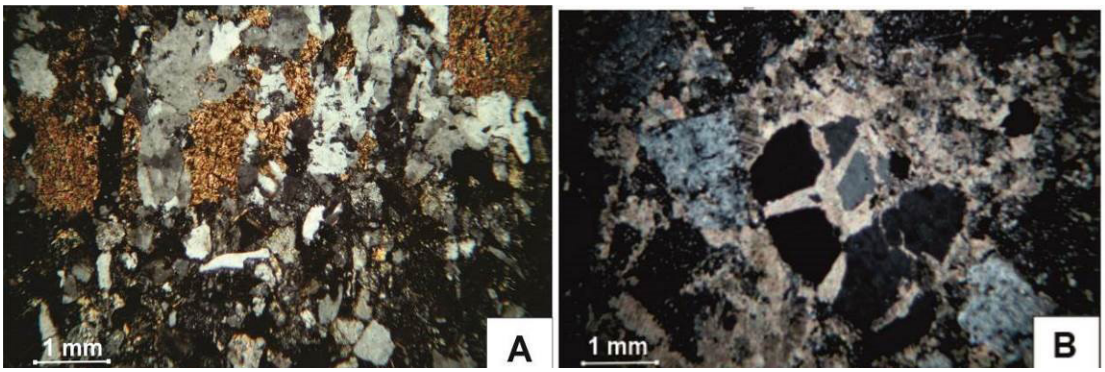

Figure 11 Photomicrographs using crossed polars. (A) PF1: Arkosic sandstone (B) PF2: Litharenite sandstone.

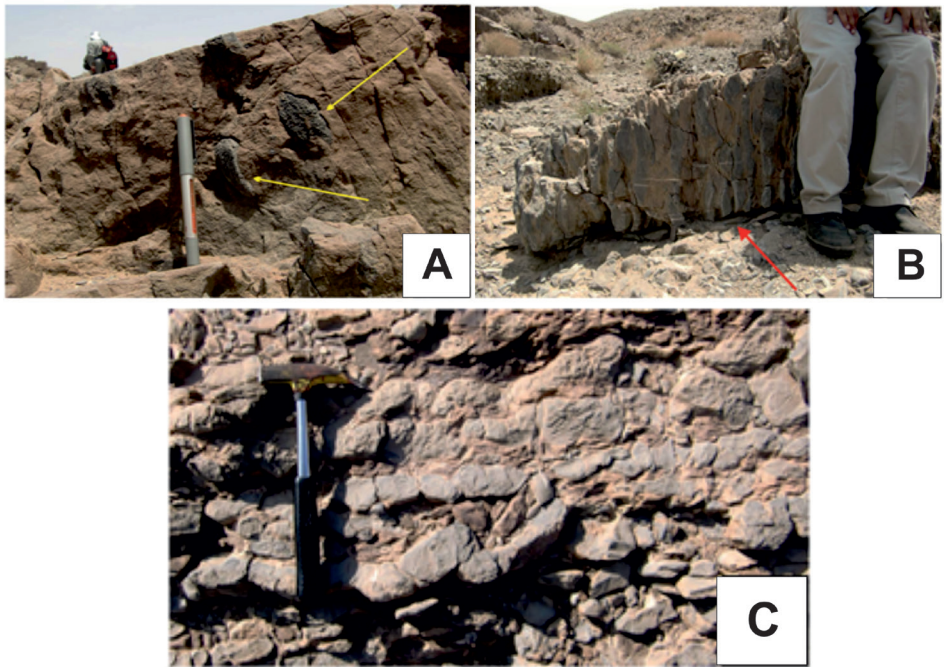

Figure 12 (A) The presence of Amonit macrofossils in carbonate units. (B) and (C) Hemipellagic carbonate sediments in intermittence with shale with boudinage structure.

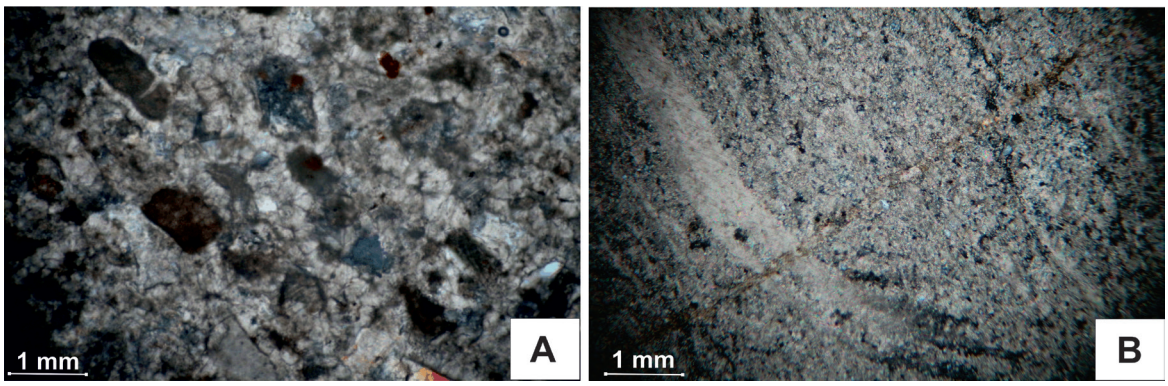

Figure 13 Photomicrographs using crossed polars. (A) MF3: Sandy intraclast wackestone/packstone. (B) MF4: mudstone.

http://dx.doi.org/10.18268/BSGM2023v75n2a070323

medium sandstone of the layer (Units 13, 15, 18, 20, 21, 22, 23). In thin section, this microfacies has a fracture which is filled with coarse-grained calcite. Clastic fine-grained quartz particles are found in the matrix of this facies. In some thin sections, the lime microcrystalline matrix is converted into microcrystalline dolomite. In addition, the remnants of bivalves replaced by calcite are found in this facies. Mudstones existing above the section indicate the remnants of very fine dolomitization (Figure 13B).

Interpretation: The presence of slumping and boudinage structures in this sequence indicates the formation of these facies in the deep slope environment of the continent (Cojan and Renard, 2020). Other evidence suggests the presence of ammonoid macrofossils in these units, which is specific to the deep environment (Page, 2008). This microfacies can be equivalent to the standard facies SMF4 (Wilson, 1975) and belongs to the facies zone as FZ1 or FZ3 (Wilson, 1975; Flugel, 2010).

4.2.2.2. Clastic facies

L2: Mud-supported conglomerate: Lithofacies L2 is a mud-supported conglomerate in the middle section of the Alam formation as thin , thick and massive bedding to lens-like layers between the sand layers. It has gravels with a diameter of 2 to 15 cm and its gravel content is about 30%. The thickness of the conglomerate layers is about 1 m, which are in the form of strips between the sandstones. The constituent grains are generally angled and have poor alignment. Gravels of this lithofacies sometimes show semi-parallel and sometimes parallel imbrication with bedding (Figure 14).

Interpretation: Poor sorting and the absence of sedimentary structures along with irregular imbrication indicate deposition by turbidity flow (lowey, 2007; Mueller *et al.*, 2017). This evidence shows the turbulence of flow before sedimentation, and a drag during sedimentation. This facies can be seen as a representation of the sedimentation of bed load (drag bed) from the low part of a layered turbidity flow (Thomas, 2011). This facies corresponds to lithofacies Fa-1 (Thomas, 2011), LF2 (Casciano *et al.*, 2019) and FA4 (Riahi *et al.*, 2010).

L3: Pebble coarse-grained sandstone facies: This facies is sandstone and sometimes its pebble content is calcareous and sometimes volcanic and metamorphic. In this lithofacies, there are scattered pebbles whose diameter is generally between 3 and 4 cm. This lithofacies exist like calcareous sandstone and has a very light brown color to dark brown with laminations and dolomitized fractures. Moreover, fine-grained conglomerate lenses with a diameter

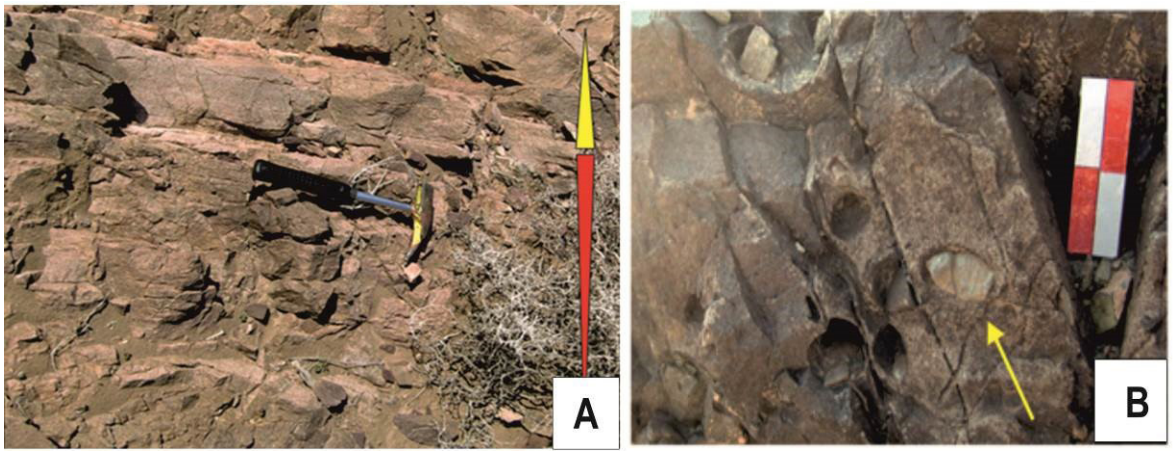

Figure 14 (A) Intermittence of conglomerate and limestone. Red triangle: succession of coarse-upward and the presence of imbrication in conglomerate lithofacies. Yellow triangle: succession of thinning-upward in limestone. (B) The conglomerate units have rounded calcareous clasts and the cavities result from the erosion of these clasts. Scale equals 10 cm.

http://dx.doi.org/10.18268/BSGM2023v75n2a070323

of 30 to 40 cm and a thickness of 1 cm were observed. The thickness of the layers reaches more than 50 cm. Cavitation erosion has eliminated pebbles. Sometimes, this facies has lenses with a flat base at the top and a curved base at the bottom (Figure 15). In addition, their construction is like cross-bedding classification and works of ripple marks, similar to LF2 (Casciano *et al.*, 2019) and FA3 (Riahi *et al.*, 2010).

Interpretation: This facies is somewhat similar to the B2 facies of Numidian sandstone (Pinter *et al.*, 2016), which was formed by deposition along the main axis of the turbidity flow. The plate-shaped nature of the layers in this facies indicates that they were not confined to a specific channel, but rather stacked on top of each other to form highly elongated lobes (Pinter *et al.*, 2016).

L4: medium-grained sandstone lithofacies to thin-layer siltstone: This facies is the most abundant among clastic facies. It has tensile sedimentary structures and the constructions of normal granulation (Ta), parallel lamination (Tb), and cross-bedding lamination (Tc). It has several within shale, limestone, and deformed structures. The layers consist of fine- to large-laminated sandstones and ripple interlayer (Tb and Tc, respectively, Bouma cycle) with shale (hemiplegic shale and Te) (Figure 16).

Interpretation: Normal gradual granulation with tensile structures indicates turbulent flows in which the intensity of turbulence is reduced and stagnant (Bouma, 1962). Lens and tabular lamination, sedimentary structures resulting from fluid escape, and deformed structures have been observed occur together as sedimentation in this association. This facies corresponds to FA-3 lithofacies (Thomas, 2011) and is similar to LF6 facies (Casciano *et al.*, 2019).

L5: shale: The facies, in the Alam Formation, consists of thin to medium layers (less than 30 cm) and is sometimes thick(up to 50 cm). There are the gradual granulation and sequencing of Buma, Te-d, and slumpling structures among its important sedimentary structures. In most cases, shale and siltstone bedding of this facies are completely delaminated. The deposits of this facies are silt and clay in size, and there are also thin interlayers

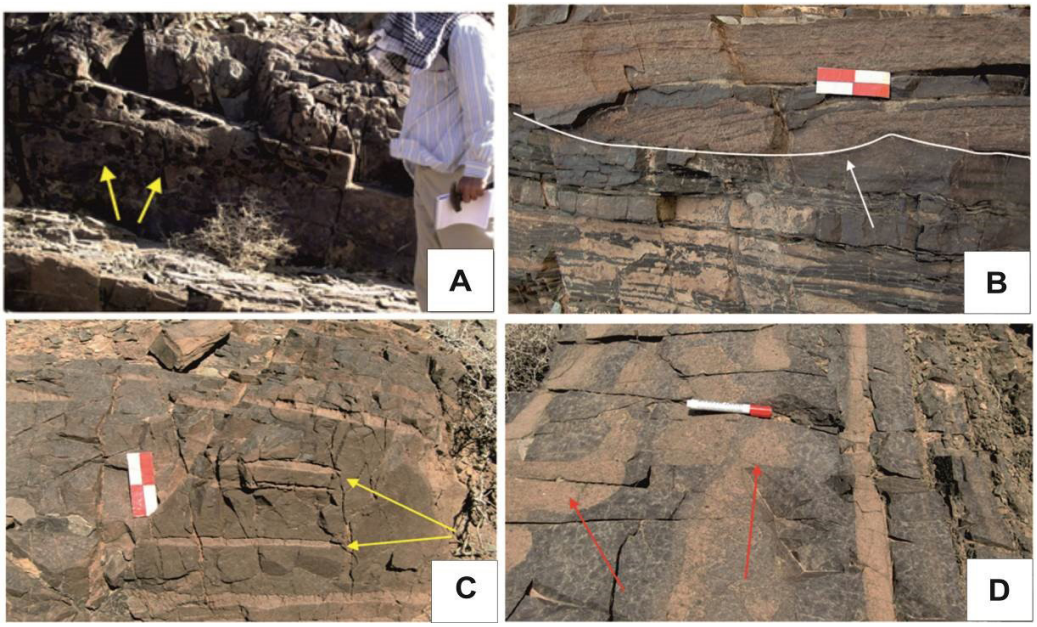

Figure 15 Data (A) Erosion of cavities caused by the removal of pebbles in the groundmass of coarse sandstones. (B) The boundary of the loaded limestone units and shale at the bottom, with large conglomerate lenses and coarse-grained sandstone with calcareous background and polygenic clasts. (C) Sandstone with lenses with flat base (top) and curved base (bottom). (D) Interlayers of sandstone containing coarse-grained pebbles.

http://dx.doi.org/10.18268/BSGM2023v75n2a070323

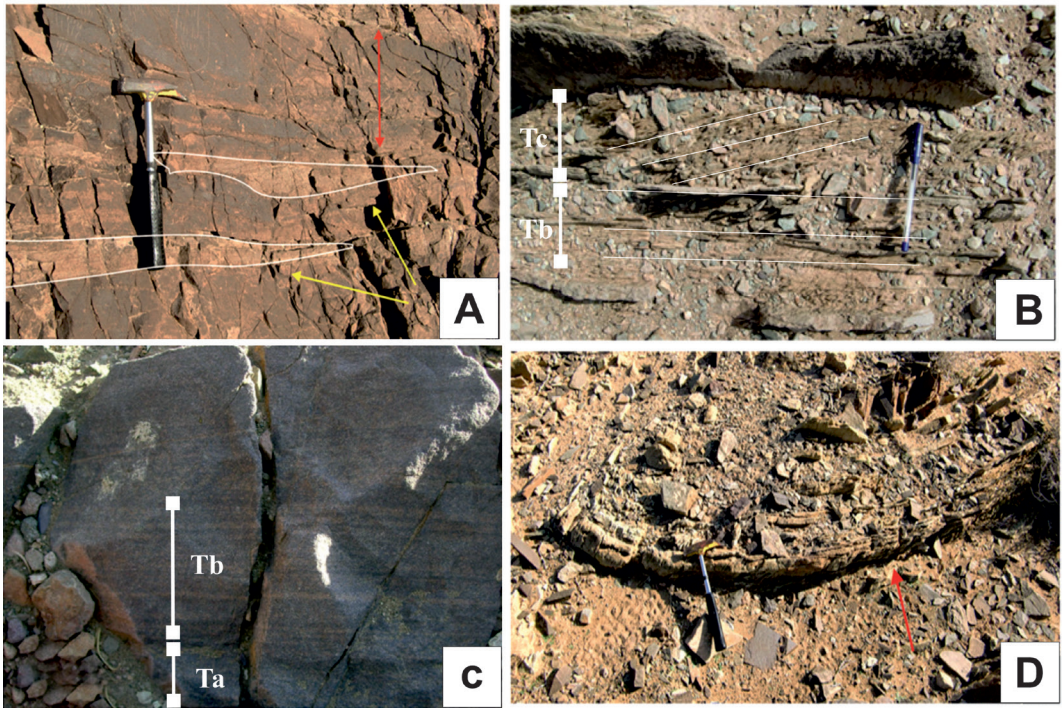

Figure 16 (A) Destroyed calcareous horizons with yellow to orange color (yellow arrow) in dark yellow sandstone (red arrow). Thick layer of sandstone with black weathering surfaces and fresh yellow surfaces. (B) Sandstone with parallel lamination (Tb) and cross-bedding lamination (Tc). (C) Sandstone with normal granulation (Ta) and cross-bedding lamination (Tc). (D) Erosional channels.

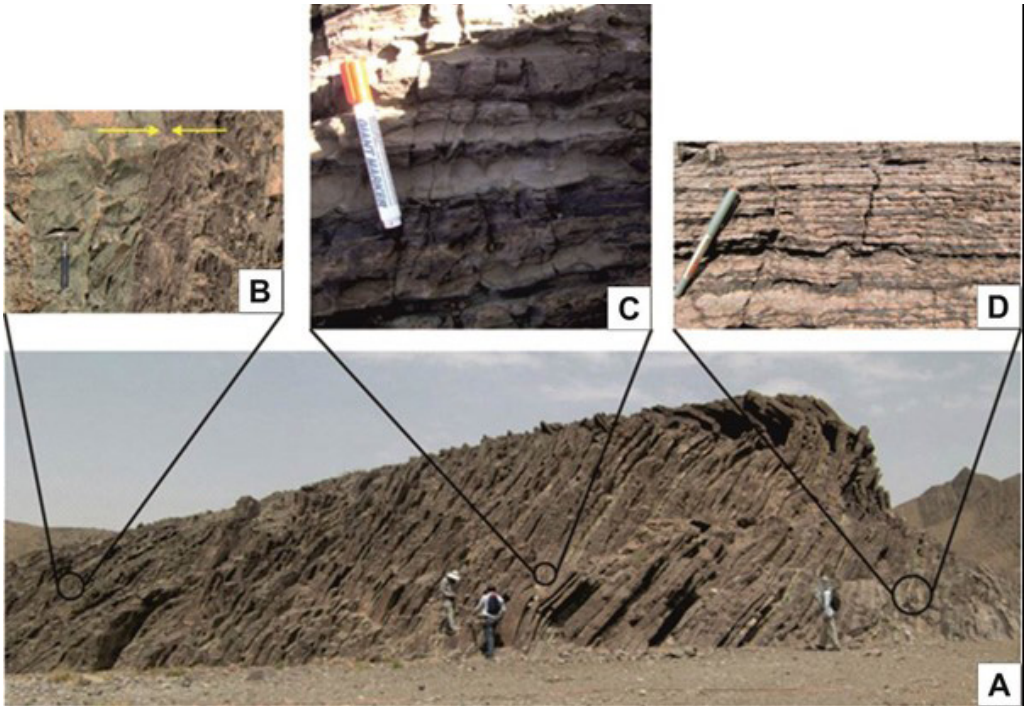

Figure 17 (A) Units deposited in maximum depth of basin with succession of clay–lime. (B) Boundary of green shale and purple shale. (C) Intermittence of clay and lime related to deep parts of the basin. (D) Succession of clay and lime in upper parts of the section with thinner and regular layers.

of sandstone and limestone. Sometimes, this lithofacies is seen as a cycle with layers of sandstone and sometimes with limestone layers (Figure 17).

Interpretation: This facies represents the deposition of very thin flows, which was most likely the result of a lateral overflow above the main turbidity flow channel that was discharged into this part of the basin before arriving at the main sandstone flow (Pinter *et al*., 2016). This lithofacies is similar to that of FA1 (Riahi *et al*., 2010) and F12 (Casciano *et al*., 2019).

Petrography of clastic facies

Clastic petrofacies in this set includes polymictic conglomerate petrofacies, sandstone petrofacies, and shale. The sandstone composition of this sequence is based on the Folk triangle arkosic sandstone, subarkose sandstone, Lithic arkose sandstone, and Litharenite sandstone (Figure18). Characteristics of these petrofacies are as follows:

PF3: Arkosic sandstone: It is found in the form of sandstone in intermittence with shale. They are brown to black sandstone with light gray weathered surface (Units 10, 20, 22, 23). The quartz content of this petrofacies is between 43% and 76%, the feldspar is between 19% and 50%, and the amount of lithic fragments is between 4% and 8%. The size of quartz grains is between 0.07 and 0.1 mm, their sorting status is in the limit of medium to good, and their roundness is weak. The arkosic sandstone facies are more coarse-grained than the arkosic sandstone facies of association A. Their veins are sometimes filled with ferrous materials and secondary quartz (Figure 19A).

PF4: Subarkose sandstone: They are black on weathered surfaces and light gray-black on fresh surfaces (Units 17, 19, 20, 22). The quartz content of this petrofacies is 82%, the feldspar is 16%, and the amount of lithic fragments is 2%. The size of fine to medium particles is 0.5 to 0.05 mm and they have weak roundness and immature sorting. Chlorite and muscovite minerals can be visible at the top of the section in this microfacies (Figure 19B).

PF5: Lithic arkose sandstone: They are in the form of repetitive cycles and have laminae in intermittence with shale layers (Units 17, 19, 20, 22). The

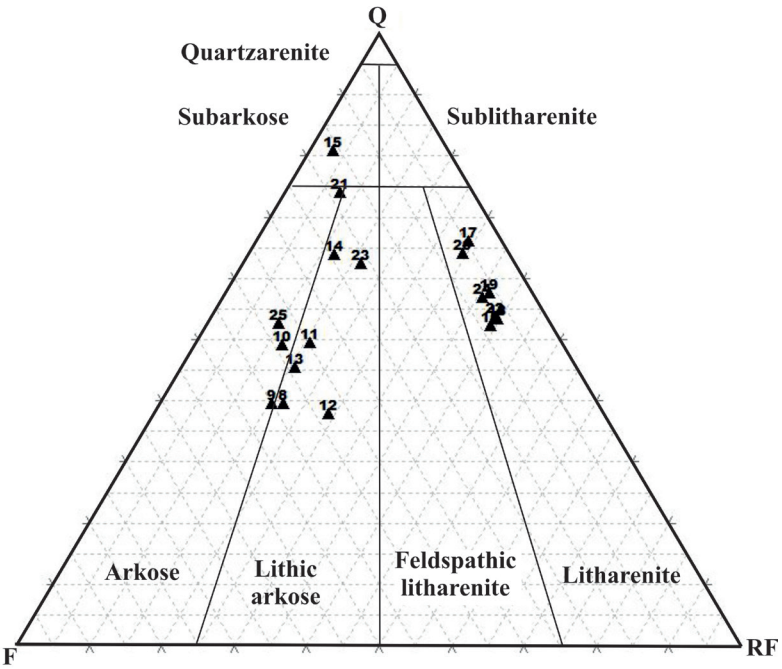

Figure 18 Data of facies association B on the sandstone classification on a QFR diagram(Folk, 1980).

http://dx.doi.org/10.18268/BSGM2023v75n2a070323

quartz content of this petrofacies is between 40% and 68%, the feldspar is between 23% and 46%, and the amount of lithic fragments is between 8% and 18%. The size of particles is medium to fine, and they have weak roundness, low sorting, and immature texture. Silica cements are syntaxial and carbonate cements are blocky and poikilotopic around clastic particles (Figure 19C).

PF6: Litharenite sandstone: PF6 consists of layered sandstones and fining upward sandstones, along with different coarse-grained horizons of 40 to 50 mm with cavitation erosion In addition, this petrofacies is in alternation with shale and thickening upward layers on the field (Units 17, 20, 22, 23). The grains mainly include quartz, feldspar, and rock fragments. The quartz content of this petrofacies is between 56% and 74%, the feldspar is between 5% and 9%, and the amount of lithic fragments is between 20% and 37%. The size of particles is fine to medium, and they have low roundness and weak sorting. Fine-grained quartz grains have a size of 0.1 mm, are sub-angular, and have medium sorting. PF6 has more immature texture than lithic arenite sandstone in facies association A. (Figure 19D).

PF7: Polymictic conglomerate: PF7 is relatively thin stripes among the sandstone layer, which is lighter color than the encompassing sandstones (Units 10 and 20). Clasts are between 3 and 5 mm in field measurements with a grain size of 0.5 to 3 mm in laboratory measurements. The constituent particles are mostly feldspar, quartz, and rock fragment. Rock fragments of this petrofacies are mostly limestone, metamorphic, and pyroclastic. The particles of this facies are angular and have weak sorting. Clastic particles are corroded, around which there is blocky calcite cement and isopachous cement. Limited fractures filled with carbonate, as well as more metamorphic rock fragments, are among the characteristics of petrofacies (Figure 20A).

PF8: Shale: PF8 has purple color, which is green in upper units (Units 10, 11, 13, 20, 21, 23). Furthermore, clastic particles are sometimes found (Figure 20B).

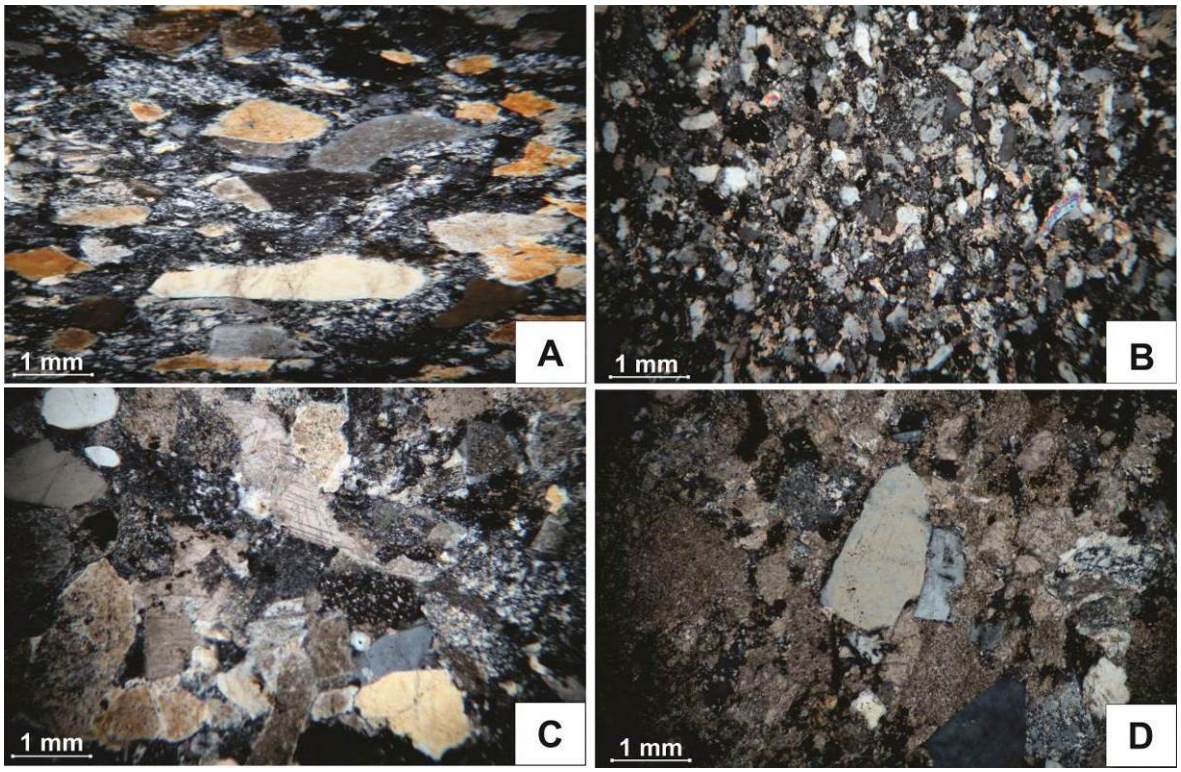

Figure 19 **Photomicrographs with crossed polars. (A) PF3: Arkosic sandstone. (B) PF4: Subarkose sandstone. (C) PF5: Lithic arkose sandstone. (D) PF6 Litharenite sandstone.**

http://dx.doi.org/10.18268/BSGM2023v75n2a070323

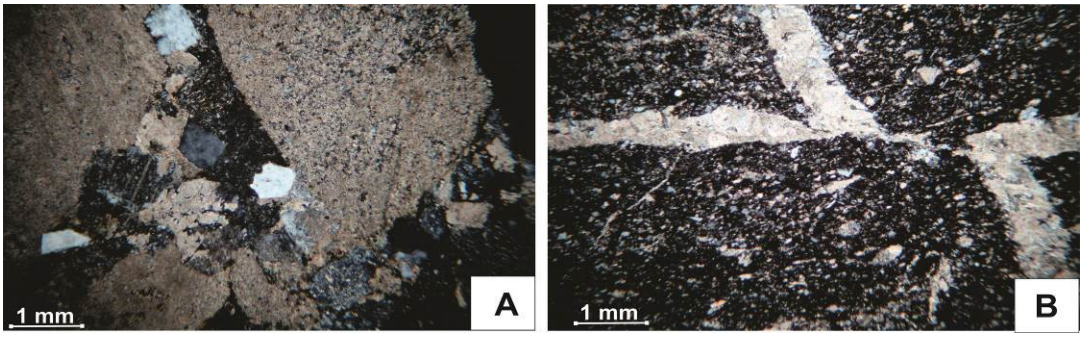

Figure 20 Photomicrographs using crossed polars. (A) PF7: Polymictic conglomerate. (B) PF7: Shale.

4.3. SEDIMENTARY ENVIRONMENT

The identified facies zones based on carbonate facies and facies associations of siliciclastic sediments indicate that the major part of the Alam Formation were deposited on the deep parts of the basin and some of its parts were deposited in the shallower parts of the platform. The tuffite layers at the bottom of the Alam Formation were replaced by thick layers of limestone. Clean limestone layers containing abundant ooids were deposited on the platform margin sand shoals. Indeed, the bottom of the Alam Formation indicates that the entrance of clastic volcanic material into the basin had stopped and that conditions were provided for depositing carbonate facies. Also, the L1 fine-grained sandstone facies was deposited in the intertidal zone in the stages of overcoming erosion on deposits and regression of the basin, as well as the conversion of the constructive shore into a destructive type in a short period of time. In addition, in stages with medium energy, limestone rocks were deposited with lamination and cross-bedding lamination (Tucker and Wright, 1990).

In general, calcareous facies indicates the stages of stagnation and the presence of shallow carbonated conditions, and the clastic facies indicates destructive stages. The presence of thin layer tuff in the base of these sediments can represent local and low-impact traction phases. These sediments have sedimentary structures belonging to high-energy conditions including cross-bedding. They also have a considerable amount of ooid in oolitic grainstone facies, which clearly represents the formation of this section in low depth and high-energy environments (Flugle, 2010). This carbonate facies includes oolitic grainstone and intraclast packstone-grainstones. These types of facies with sorted particles and the presence of ooids indicate sand shoal margins of the shelf (Flugel 2010). These barrier facies are similar to the Elika Formation in Alborz, as studied by Lasemi *et al* (2000) and Sotuhian (2008). The clastic facies set A including conglomerate, arkose sandstone, lime sandstone, and shale represents the low-depth clastic sea. Sandstone facies were deposited in the phases of dominating erosion and the regression of the basin and when the inactive shore was converted to an active shore (Tucker and Wright, 1990). These sandstone facies, in the high-energy condition, were deposited in the intertidal limit (Tucker and Wright, 1990).

Entrance of the clastic particles to the intertidal limit can be related to coastal flows, sudden storms, and/or tectonic activities on the provenance of the silica-clastic sediments (Flugel, 2010). Polymictic conglomerate petrofacies in this facies association represents high-energy positions while passing stationary phases to high-energy phases and indicates high-energy erosive channel sub-environment (Collinson and Thompson, 1987). Totally, packstone facies indicate stationary stages and the presence of low-depth carbonate conditions, and grainstone and sandstone facies indicate the destructive phases. The transected section of

http://dx.doi.org/10.18268/BSGM2023v75n2a070323

association A is demonstrated in Figure 21. Dark and purple sandstone layers containing Lithofacies L4 were deposited on these carbonates. This sequence also has limestone interlayers.

Then, the conglomerate layers (L2) and the Pebble sandstones (L3) were deposited and the sediments of this lithofacies were in connection with the fine streams in the submarine fan channels (Nomar, 1970; Riccliucchi, 1974). Lithofacies L5 was intermittently deposited with the calcareous deposits. The deposit of this facies indicates the sediment of very thin currents and slumping construction is seen in this sequence. According to Stow (2005), this construction is seen in the middle lobes of the fan, so it can be said that the Lithofacies mentioned in the lobe (medial fan lobe deposit) are located in the middle of the fan. The sequence of facies set B was then deposited, which includes clastic facies such as polymictic conglomerate, arkose sandstone, litharenite sandstone, shale, and carbonate facies including mudstone and wackestone. This set was deposited in different conditions from A and the primary sequence of the formation, i.e., facies set A, and indicates deep environment and turbidity system and submarine fan. Sedimentary structures of clastic units of this facies set include layering, coarsening upward, fining upward, thickening upward, thinning upward, slumping, and slump structures (Figure 22). These facies lack structures such as cross-bedding. Chaos and disorders are more frequent and most facies are immature in terms of texture. The conglomerate of this sequence constitutes pebbles. Parts of its lower beds reduce in thickness laterally, and it has some structures such as gradual granulation, which indicates submarine channels in the continental slope area (Nichols, 2009). These polymictic conglomerate layers have metamorphic, pyroclastic, and sedimentary rock fragments that have lime matrix and indicate Shelf Canyon (Nichols, 2009; Weimer, 2004).

The set of the shale-sandstone unit facies with shale dominance over the sandstone indicates the distal parts of the outer lobe, sandstone-shale period with almost equal ratio in the deep middle lobe, and period of sandstone-shale with sandstone dominance. Also, more coarse-grained units were deposited on top of the inner lobe of a submarine fan (Stow, 2005) (Figure 23). The contents of the turbidity channels include gravel, mud, sand, or their mixture. This important case depends on some factors such as tectonics, climate, and sedimentary load (Reading and Richards, 1994; Richards *et al.*, 1998). Shale sequence with the interbedded lime in the distal parts is found in the outer lobe deposited in high depth (Stow, 2005). Sequence of shale–sandstone is dominated by distal fan special shale (Stow, 2005), which belongs to the ocean bed. This lime facies is carried by older units which are carried by the turbidity flow.

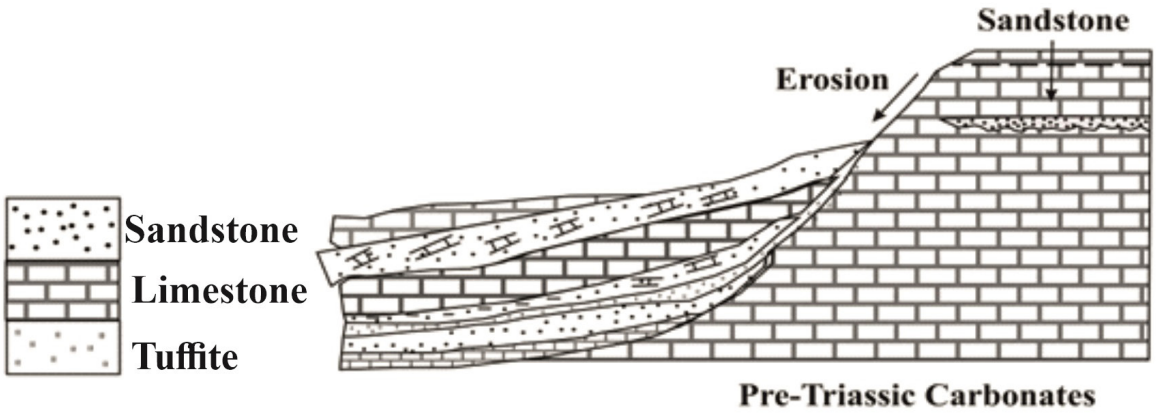

Figure 21 Transected section of the model provided for association A.

http://dx.doi.org/10.18268/BSGM2023v75n2a070323

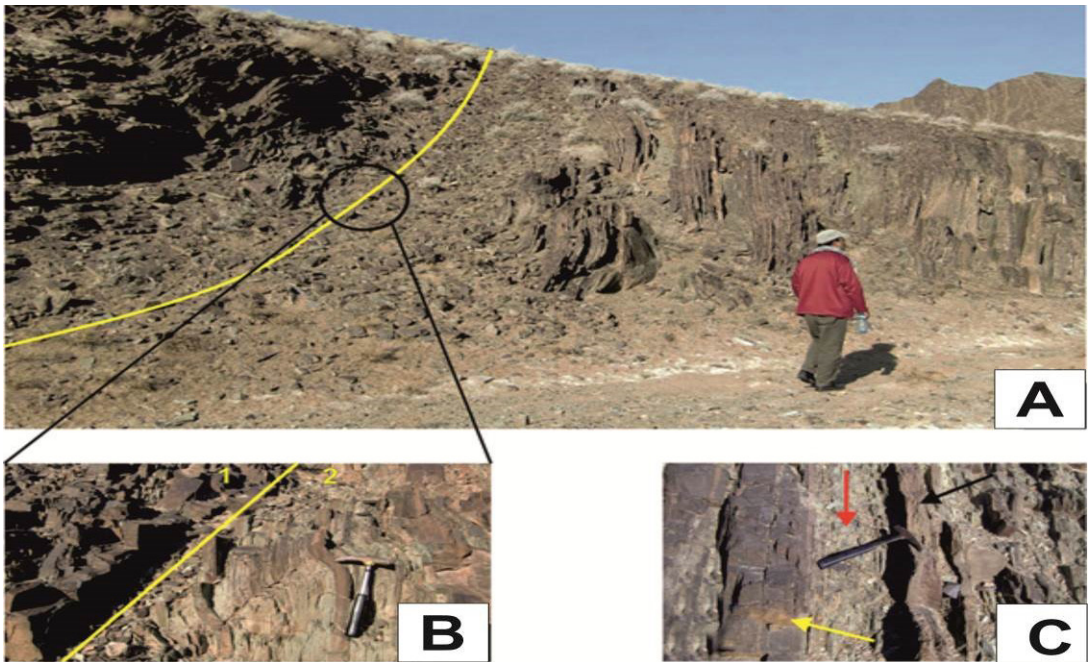

Figure 22 (A) The slope change of layers at the boundary of deep lime-clay units of the basin with the slumping structure, at the beginning of the turbidite units and at the beginning of the regression cycle. (B) 1. Deep lime-clay of the basin. 2. Limestone-sandstone-shaly limestone at the beginning of regression. (C) Succession of calcarenite sandstone and shaly limestone. Yellow arrow: calcarenite with black weathering surface and fresh surface with orange color. Red arrow: black limestone shales Black arrow: calcarenite sandstone

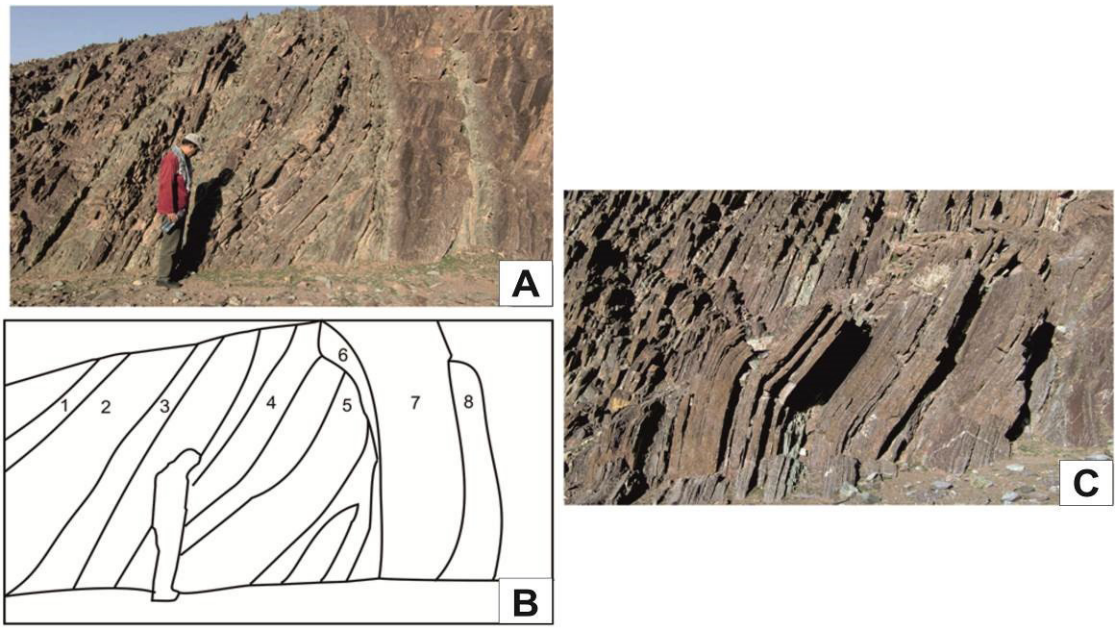

Figure 23 (A) and (B) Intermittence of purple lime-shale, green shale, and fine sand. 1. Succession of sandstone shale with dominant sandstone. 2. Alternation of sandstone-shale with dominant shale in purple and green color. 3. Intermittent layers of sandstone with a thickness of 8 to 10 cm. 4 and 5. Sandstone-shale layers with turbulence and curved boundary ending in succession of deep clay-lime. 7 and 8. Alternation of deep lime-clay units. (C) Succession of deep lime-clay in the deepest part of the basin with turbulence and folding resulting from slumping.

http://dx.doi.org/10.18268/BSGM2023v75n2a070323

These carbonates almost have lithoclast due to their combination with metamorphic or pyroclastic lithoclasts and structures such as cross-bedding and gradual granulation, and accompany rounded intraclasts and extraclasts. Sometimes, syntaxial cement indicates transportation and turbulent phases in the basin (Flugel, 2010).

Carbonates at the top of the section, which are the last sediments of Alam formation, do not have continental terrace but allodapic carbonates. These facies were deposited in the continental slope or deeper basin. These carbonates resulted from the repeated movement of carbonate sands in the continental terraces that move toward the basin as the turbidite forming lime (Flugel, 2010). These carbonates resulted from submarine erosion and have clasts in different sizes (Pinter, 2016). Intraclast grainstone facies indicates the base bed for turbidity movements and all turbulent units cause erosion grooves during the stages of turbidite slumps. Carbonate sequences were deposited in front of the continental slope and below proximal fans from a submarine fan (Stow, 2005; Nichols, 2009). The periodicity of deep clay facies and pelagic lime with slumping and boudinage structures indicates the deepest point in the deep marine environment. In association B, turbidite units are observed as compensatory cycles (Figure 24).

In addition, the sand content is high, and shale in the marine fan indicates that this fan is a sand–mud mixture in the classification proposed by Reading and Richards (1994) and Nichols (2009). The sand content of these fans is between 30% and 70% (Reading and Richards, 1994; Nichols, 2009). On the distal shaly limes of facies set B, the conglomerate of Baqoroq Formation has an erosive border indicating uplift and start of erosion in the basin. The transected section of association B is illustrated in Figure 25.

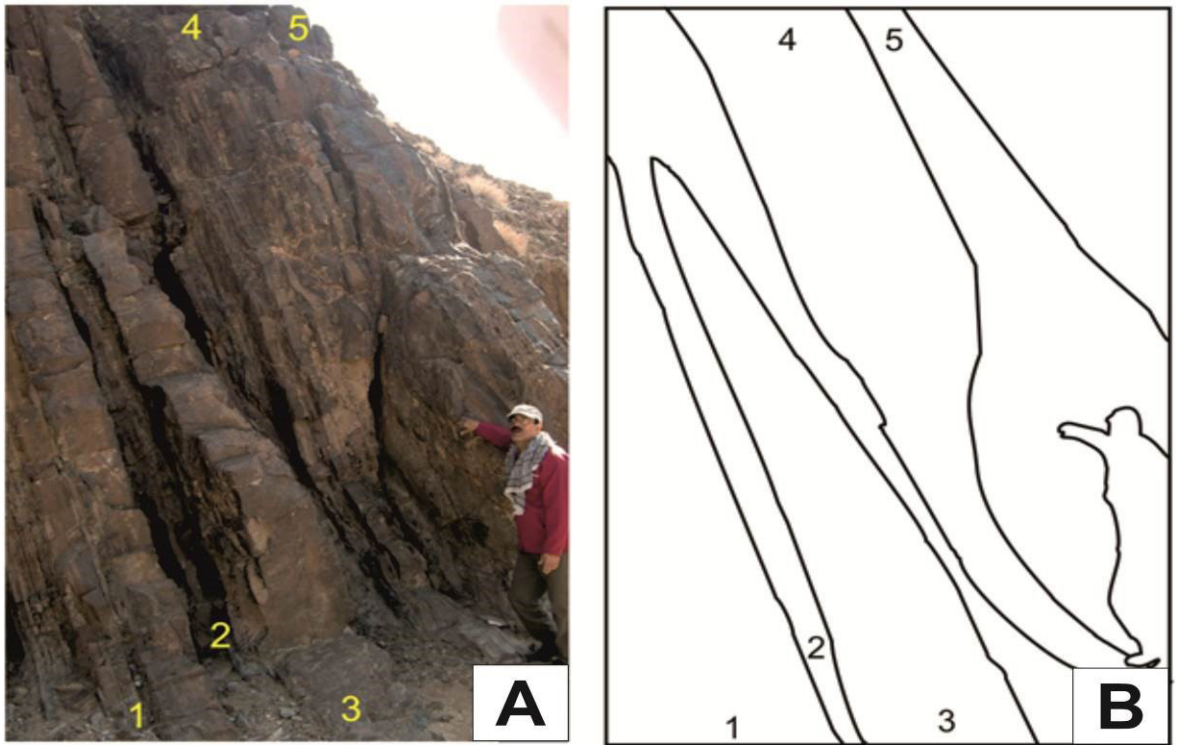

Figure 24 Loaded turbidite units in compensatory cycles. 1,3 and 4. Center of slumping lobes in compensatory cycles. 2 and 5. The edge of the slumping lobes in the compensatory cycles. At the end of lobe 3, fractures resulting from tectonics are observed.

http://dx.doi.org/10.18268/BSGM2023v75n2a070323

Considering the age of these sediments, which is Middle–Early Triassic, and the effect of early Cimmerian orogeny in Central Iran as old as the late Triassic period, the structural changes of these sediments cannot be related to the effect of early Cimmerian orogeny. However, it is evident that the sediments were effective in two major phases during sedimentation. The first phase of these sediments formed a rift in the submarine base resulting in the sedimentation of the primary deposits of the formation and changing a low-depth mixed siliciclastic-carbonate environment into the deep environment with turbidite deposits. The second phase occured with uplift and erosion, and change in a deep environment with the deposition of the turbidite deposits into a marginal shore to a continental shore (Baqoroq Formation). Thus, facies set A was deposited in a mixed siliciclastic-carbonate ramp. Facies and the similar environment of this set were reported in the study of Azami *et al.* (2012) on the Jurassic Mozduran Formation, and Seyedmehdi *et al.* (2016) on Devonian–Tournasian sediments of mixed siliciclastic-carbonate ramp of Caning Basin in Australia. Furthermore, facies set B is a deep marine sequence including turbidite deposits related to the submarine fans made from the mud-sand mixture. The sedimentary environment of these deposits found in the deep and turbiditie stage is similar to turbidity deposits of the Karaj Formation in Iran and California borderland in the United States (Covault and Romans, 2009) and the Langjiexue group located in southern Tibet (Zhang *et al.*, 2015). A model of sedimentary environments in upper Olenekian-Anisian deposits (Alam Formation) is shown in Figure 26.

5. Conclusions

Alam Formation in Nakhlek Group in Iran is one of the deposits with the age of Upper Olenekian-Anisian ,with a thickness of 720 m, has a lithology of sandstone, shale, limestone, and pyroclastic units. At the beginning of the Mesozoic era and following the changes due to the effect of tectonic events, sedimentary environments were affected by these events and rearranged after a series of

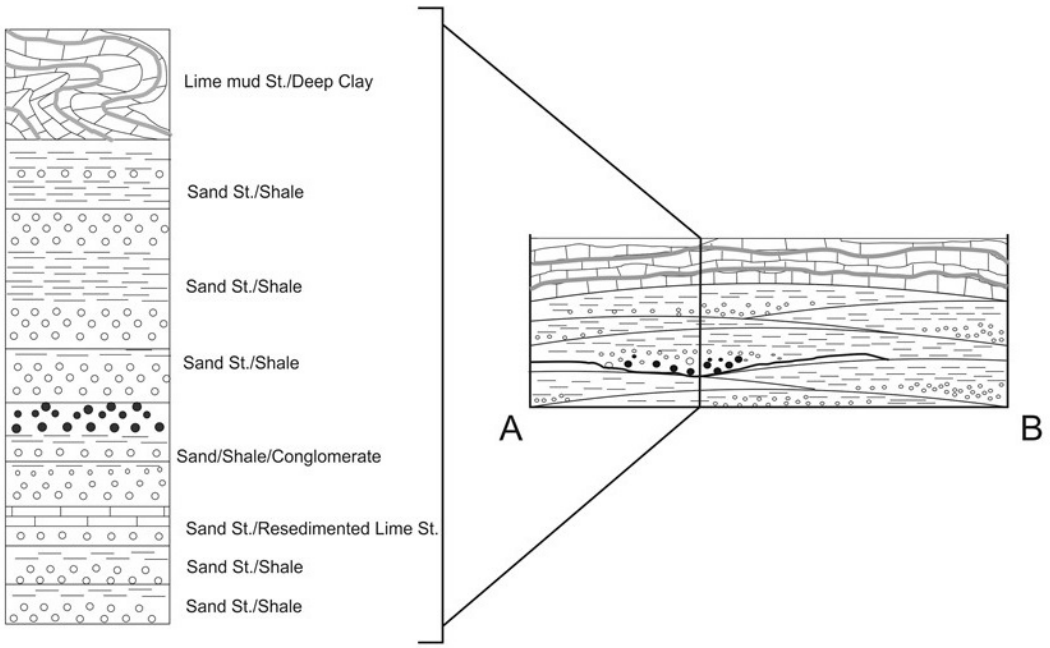

Figure 25 Transected section of the model provided for association B. (St: stone).

http://dx.doi.org/10.18268/BSGM2023v75n2a070323

turbulence. These tectonic activities left a significant impact on the sediments of this depositional environment. After tensile movement, the basin was periodically converted from a stable shallow sea with carbonate deposits to clastic basins dominated by clastic sedimentation. Thus, the basin has become a shallow-clastic-carbonatee sea. The result of such an environment is the deposits of lime, sandstone, shale, sandy lime, and calcareous sandstone, leading to over-carbonate sediment in the stages of the marine progression and over-clastic sediment in the stage of marine regression. The clastic facies of this association consists of fine-grained sandstone, which, based on the composition of the grains, includes the two petrofacies of arkosic sandstone and litharenite sandstone. The calcareous facies in association A are characterized by two microfacies consisting of oolitic grainstone and intraclast oolitic packstone/grainstone. Furthermore, tuffitie is the only pyroclastic facies. This sequence was introduced in the form of a facies collection A. Then, due to the increase in sediment load entering the basin and the depth in the basin, a large volume of sedimentary deposits entered the basin, leading to the formation of a deep turbidity environment deposited on a steep bed (continental slope). The resulting sedimentary rows included the sequences of conglomerate, sandstone, and shale, which were deposited after the relative stability and sedimentation of limes in intermittence with deep clay deposits. The effect of regression was followed by creating turbidity deposits in the second phase in the basin and clastic facies, such as conglomerate, pebble coarse-grained sandstone, medium-grained sandstone to thin layer siltstone, and shale lithofacies. The lithological composition of such a turbidity includes polymictic conglomerate, arkosic sandstone, sub arkose sandstone, lithic arkose, litharenite sandstone, and shale. The carbonate facies consists of two microfacies such as sandy intraclastic wackestone/packstone and mudstone and the last step of regression was ended with conglomerate deposits on the boundary of the Baqoroq Formation. Based on the results, the environment of this formation was shallow-deep carbonate-silica marine, as well as the deposits of deep-sea channels and horns deposited in the continental slope under the mechanism of turbidity flows.

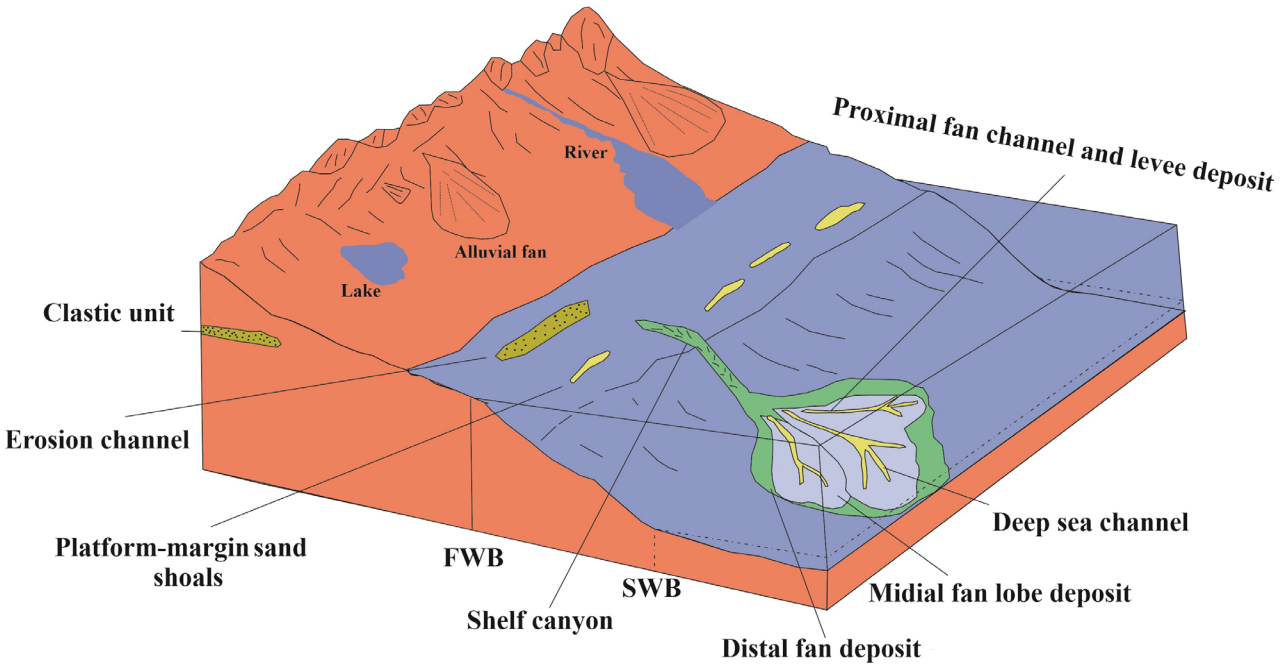

Figure 26 The model of sedimentary environments in Upper Olenekian-Anisian deposits (Alam Formation), Central Iran.

http://dx.doi.org/10.18268/BSGM2023v75n2a070323

Contributions of authors

Payman Rezaee: Conceptualization, Supervision, Validation, Reviewing and Editing. *Seyedeh Akram Jooybari:* Methodology, Software, Data curation, Writing- Original draft. *Kiamars Hosseini*: Methodology and Software. *Amin Moodii:*Sampling, Software and Data curation.

Financing

The authors declare that no funds, grants, or other support were received during the preparation of this manuscript.

Acknowledgements

The authors thank the anonymous reviewers who provided constructive comments.

Conflicts of interest

The authors have no relevant financial or non-financial interests to disclose.

Availability of data and materials

The datasets used and/or analysed during the current study are available from the corresponding author on reasonable request.

References

Annan, A., 2001, Ground Penetrating Radar Workshop Notes: Ontario, Canada, Sensors and Software, Inc., 192 p.

Alavi, M. Vaziri, H. Seyed-Emami, K., Lasemi, Y., 1997, The Triassic and associated rocks of the Nakhlak and Aghdarband areas in central and northeastern Iran as remnants of the southern Turanian active continental margin: Geological Society of America, Bulletin, 109,1563–1575. https://doi.org/10.1130/0016-7606(1997)109<1563:TTAARO>2.3.CO;2

Almasian, M., 1997, Tectonics of Anarak Area (Central Iran): Tehran, Iran, University of Azad, Ph.D. thesis, 164p.

Angiolini, L., Gaetani, M., Muttoni, G., Stephenson, M. H., Zanchi, A., 2007, Tethyan oceanic currents and climate gradients 300 m.y. ago: Geology, 35, 1071–1074. https://doi.org/10.1130/G24031A.1

Azami, H., Poorsoltani, M., Alameh, M., 2012, Study of facies and sedimentary history of Mozdaran Formation in Saleh Abad Northeast Iran: Journal of Environmental Geology, 6(19),35-48.

Bagheri, S., Stampfli,G.M., 2008, The Anarak, Jandaq and Posht-e-Badam metamorphic complexes in central Iran: New geological data, relationships and tectonic implications: Tectonophysics, 451,123-155. https://doi.org/10.1016/j.tecto.2007.11.047

Balini, M., Nicora, A., Berra, F., Garzanti, E., Levera, M., Mattei, M., Muttoni, G., Zanchi, A., Bollati, I., Larghi, C., Zanchetta, Salamati, R., Mossavvari, F., 2009, The Triassic stratigraphic succession of Nakhlak (Central Iran), a record from an active margin, in Brunet, M.-F., Wilmsen, M., Granath, J. W., (eds.), South Caspian to Central Iran Basins: London, The Geological Society, Special Publications, 312, 287–321. https://doi.org/10.1144/SP312.14

Bouma, A.H., 1962, Sedimentology of some Flysch deposits: A graphic approach to facies interpretation: Amsterdam, Elsevier, 168p.

Brunet, M.F., Korotaev, M.V., Ershov, A.V., Nikishin, A.M., 2003, The South Caspian Basin: a review of its evolution from subsidence modelling: Sedimentary Geology, 156, 119–148. https://doi.org/10.1016/S0037-0738(02)00285-3

Catuneanu, O., 2006, Principles of sequence stratigraphy, Amsterdam, Elsevier, 398p.

Casciano, C.I., Patacci, M., Longhitano, S. G., Tropeano, M., McCaffrey, W.D., Di Celma,

C., 2019, Multi-scale analysis of a migrating submarine channel system in a tectonically-confined basin: The Miocene Gorgoglione Flysch Formation, southern Italy: Sedimentology, 66(1), 205-240. https://doi.org/10.1111/sed.12490

Coe, A.L., 2003, The sedimentary record of sea-level change: Cambridge, Cambridge University Press, 452p.

Cojan, I., Renard, M., 2020, Sedimentology: London, Routledge, 492 pp.

Covault, J., Romans, B., 2009, Growth patterns of deep-sea fans revisited: Turbidite system morphology in confined basins, examples from the California Borderland: Marine Geology, 265, 51–66. https://doi.org/10.1016/j.margeo.2009.06.016

Davoudzadeh, M., Schmidt, K, 1981, Contribution to The Paleogeography and Stratigraphy of the Upper Triassic to Middle Jurassic of Dan: Neues Jahrbuch für Geologie und Paläontologie, 162(21),137-163.

Davoudzadeh, M., Seyed-Emami, K., 1972, Stratigraphy of the Triassic Nakhlak Group, Anarak Region, Central lran: Geological Survey of Iran, 28, 1- 28.

Davoudzadeh, M., Soffel, H., Schmidt, K., 1981, On the rotation of lhe Central-East-han microplate. Neues Jahrbuch für Geologie und Paläontologie, 3,180-192. https://doi.org/10.1127/njgpm/1981/1981/180

Dercourt, J., Gaetani, M., Vrielynck, B., BarrierBiju-Duval, B., Brunet, M.F., Cadet, J.P., Crasquin, S., Sandulescu, M., 2000, Atlas Peri-Tethys Paleoegeographical Maps, vol. I-XX: Paris, Commission de la Carte Géologique du Monde, 269 p.

Dunham, R.G., 1962, Classification of carbonate rocks according to depositional texture, in Ham, W. E. (Ed.), Classification of carbonate Rocks: Canada, American Association of Petroleum Geologists, Memoir 1, 108-121.

Dickinson, W.R., Suczek, C.A., 1979, Plate tectonics and sandstone compositions: American Association of Petroleum Geologist, Bulletin, 63, 2164–2182. https://doi.org/10.1306/2F9188FB-16CE-11D7-8645000102C1865D

Einsle, O., Stach, P., MesserschmidtSimon, J., Kröger, A., Huber, R., Kroneck, P.M., 2000, Cytochrome c Nitrite Reductase from Wolinella succinogenes structure at 1.6 å resolution, inhibitor binding, and heme-packing motifs: Journal of Biological Chemistry, 275(50), 39608-39616. https://doi.org/10.1074/jbc.M006188200

Flugel, E., 2010, Microfacies of carbonate rocks ,analaysis, interpretation and application: Berlin, Springer-Verlag, 976p. https://doi.org/10.1007/978-3-642-03796-2

Folk, R.L., 1974, Petrology of sedimentary rocks: Austin, Texas, Hemphill Pub. Co., 170p.

Folk, R.L., 1980, Petrology of sedimentary rocks: Austin, Texas, Hemphill Pub. Co.,184p.

Garzanti, E., 2019, Petrographic classification of sand and sandstone: Earth-Science Reviews, 192, 545-563. https://doi.org/10.1016/j.earscirev.2018.12.014

Ghorbani, M., 2019, Lithostratigraphy of Iran: Switzerland, Springer International Publishing, 274p. https://doi.org/10.1007/978-3-030-04963-8

Hopkins, J., Wysoczanski, R.J., Orpin, A.R., Howarth, J.D., Strachan, L.J., Lunenburg, R., Camp, S., 2020, Deposition and preservation of tephra in marine sediments at the active Hikurangi subduction margin: Quaternary Science Reviews, 247, 106500. https://doi.org/10.1016/j.quascirev.2020.106500

Hashemi Azizi, S.H., 2018, Depositional conditions, diagenesis and provenance of sedimentary rocks of the "Nakhlak Group" northeast of Naein area, Central Iran: Bandar Abbas, Iran, University of Hormozgan, Ph.D. Thesis, 306p.

Hashemi Azizi, S.H., Rezaee, P., Jafarzadeh, M., Meinhold, G., Mousavi Harami, S. R., Masoodi, M., 2018, Early Mesozoic sedimentary–tectonic evolution of the Central-East Iranian Microcontinent:

Evidence from a provenance study of the Nakhlak Group: Geochemistry, 78(3), 340-355. https://doi.org/10.1016/j.chemer.2018.06.003

Krystyn, L., Tatzreite, F., 1991, Middle Triassic ammonoids from Aghdarband (NE lran) and their paleobiogeographical significance: Acta geologica Polonica, 38, 139-163.

Lasemi, Y., Jahani, D., Kohansal Ghadimvand, N., 2000, Survey of Elika Formation in West Alborz East (Ghaznavid Region): Facies, sedimentary environments and sequence stratigraphy, in Fourth Conference of the Geological Society of Iran: Tabriz, GSI, 8p.

Lowey, G.W., 2007, Lithofacies analysis of the Dezadeash Formation (Jura Cretaceous), Yukon, Canada: The depositional architecture of a mud/sand-rich turbidite system: Sedimentary Geology, 198, 273-291. https://doi.org/10.1016/j.sedgeo.2006.12.011

Martizzi, P., Chiyonobu, S., Hibi, Y., Yamato, H., Arato, H., 2021, Middle–late Miocene paleoenvironment of the Japan sea inferred by sedimentological and geochemical characterization of coeval sedimentary rocks. Marine and Petroleum Geology, 128, 105059 . https://doi.org/10.1016/j.marpetgeo.2021.105059

Mass, J.P., Fenerci, M., Pernarcic, E., 2003, Palaebathymetric reconstruction of peritidal arbonates, Late Barremian, Urgonian, Sequences of Provence (SE France): Palaeogeography, Palaeclimatology, Palaeoecology, 200, 65-81. https://doi.org/10.1016/S0031-0182(03)00445-0

Mazzullo, S.J., 1992, Geochemical and neomorphic alteration of dolomite: a review: Carbonates and Evaporites, 7, 21-37. https://doi.org/10.1007/BF03175390

Miall, A., 2000, The geology of stratigraphic sequences: Berlin, Springer, 435p. https://doi.org/10.1007/978-3-662-03380-7

Mojsisovics, E., 1893, Faunistische Ergebnisse aus der Untersuchung der Ammoneen-faunen der Mediterranen Trias: Abhandlungen der Geologischen Reichsanstalt, 6, 810-830.

Mueller, P., Patacci, M., Di Giulio, A.M., 2017, Hybrid event beds in the proximal to distal extensive lobe domain of the coarse-grained and sand-rich Bordighera turbidite system (NW Italy): Marine and Petroleum Geology, 86, 908-931. https://doi.org/10.1016/j.marpetgeo.2017.06.047

Nichols, G., 2009, Sedimentology and stratigraphy, Second edition: UK, Wiley-Blackwell, 419p.

Nikbakht, S.T., Rezaee, P., Nasiri, Y., Moussavi-Harami, R., Khanehbad, M., 2022, Petrography and geochemistry of the Early Permian strata in the Kalmard Area, Central Iran Zone, Implications on provenance and tectonic setting: Himalayan Geology, 43(2), 417-428.

Pettijohn, F.J. Potter P.I. and Siever,R. 1987. Sand and Sandstone. 2nd ed., Springer- Verlag, New York. 553pp.

Pinter, P.R., Butler, R.W.H., Hartley, A.J., Maniscalco, R., Baldassini, N., Di Stefano, A., 2016, The Numidian of Sicily revisited: a thrust-influenced confined turbidite system: Marine and Petroleum Geology, 78, 291-311. https://doi.org/10.1016/j.marpetgeo.2016.09.014

Reading, H.G., Richards, M., 1994, Turbidite systems in deep-water basin margins classified by grain size and feeder system: AAPG bulletin, 78(5), 792-822. https://doi.org/10.1306/A25FE3BF-171B-11D7-8645000102C1865D

Rezaee, P., Khanehbad, M., Ezatifar, M., Jooybari, S.A., Hosseini, K., 2022, Facies analysis, sedimentation conditions and geochemistry of clastic deposits of Ashin formation (Late Ladinian-Early Carnian), Northeast of Nain, East of Central Iran: Iranian Journal of Earth Sciences, 14(3), 221-240. https://doi.org/10.30495/IJES.2021.685396

Riahi, S., Soussi, M., Boukhalfa, K., Ben Ismail-Lattrache, K., Stow, D., Sami, K., Mourad, B., 2009, Stratigraphy, sedimentology and

http://dx.doi.org/10.18268/BSGM2023v75n2a070323

structure of the Numidian Flysch thrust belt in northern Tunisia: Journal of African Earth Sciences, 57 (1-2), 109-126. https://doi.org/10.1016/j.jafrearsci.2009.07.016

Richards, M., Bowman, M., 1998, Submarine fans and related depositional systems II: variability in reservoir architecture and wireline log character: Marine and Petroleum Geology, 15(8), 821-839. https://doi.org/10.1016/S0264-8172(98)00042-7

Rossi, V.M., Longhitano, S.G., Mellere, D., Dalrymple, R.W., Steel, R. J., Chiarella, D., Olariu, C., 2017, Interplay of tidal and fluvial processes in an early Pleistocene, delta-fed, strait margin (Calabria, Southern Italy): Marine and Petroleum Geology, 87, 14-30. https://doi.org/10.1016/j.marpetgeo.2017.02.021

Ruttner, A.W., 1991, Geology of the Aghdarband area (Kopet Dagh, NE Iran): Abhandlungen der Geologischen Bundesanstalt, 38, 7–79.

Ruttner, A.W., 1993, Southern borderland of Triassic Laurasia in north-east Iran: Geologische Rundschau, 82,110–120. https://doi.org/10.1007/BF00563274

Seyed-Emami, K., 2003, Triassic in Iran: Facies, 48(1), 91-106. https://doi.org/10.1007/BF02667532

Şengör, A.M.C., 1979, Mid-Mesozoic closure of Permo-Triassic Tethys and its implications: Nature, 279, 590-593. https://doi.org/10.1038/279590a0

Seyedmehdi, Z., George, A.D., Tucker, M.E., 2016, Sequence development of a latest Devonian–Tournaisian distally-steepened mixed carbonate–siliciclastic ramp, Canning Basin, Australia: Sedimentary Geology, 333, 164-183. https://doi.org/10.1016/j.sedgeo.2015.12.012

Sibley, D.F., Gregg, J.M., 1987, Classification of dolomite rock textures: Journal of Sedimentary Research, 57(5),967-975. https://doi.org/10.1306/212F8CBA-2B24-11D7-8648000102C1865D

Soffel, H.C., Schmidt, S., Davoudzadeh, M., Rolf, C., 1996, New palaeomagnetic data from Central Iran and a Triassic palaeoreconstruction: Geologische Rundschau, 85(2), 293-302. https://doi.org/10.1007/BF02422235

Stampfli, G., Marcoux, J., Baud, A., 1991, Tethyan margins in space and time: Palaeogeography, Palaeoclimatology, Palaeoecology, 87(1-4), 373-409. https://doi.org/10.1016/0031-0182(91)90142-E

Stampfli, G.M., Borel, G.D., 2002, A plate tectonic model for the Paleozoic and Mesozoic constrained by dynamic plate boundaries and restored synthetic oceanic isochrons: Earth and Planetary Science Letters, 196(1-2),17-33. https://doi.org/10.1016/S0012-821X(01)00588-X

Stocklin, J., 1968, Structural history and tectonics of Iran: a review: The American Association of Petroleum Geologists, Bulletin, 52, 1229-1258. https://doi.org/10.1306/5D25C4A5-16C1-11D7-8645000102C1865D

Stow, D., 2005, Sedimentary rocks in the field. A colour guide: England, Manson Publishing Ltd., 320p.

Torsvik, T.H., Cocks, L.R.M., 2004, Earth geography from 400 to 250 Ma: A palaeomagnetic, faunal and facies review: Journal of the Geological Society of London, 161(4), 555-572. https://doi.org/10.1144/0016-764903-098

Thomas, M.F.H., 2011, Sedimentology and basin context of the Numidian Flysch Formation; Sicily and Tunisia: England, University of Manchester, Ph.D. Thesis, 278p.

Tozer, E., 1972, Triassic Ammonoids and Daonella from the Nakhlak Group, Anarak Region, Central Iran: Geological Survey of Iran, 235, 1156-1166.

Tucker, M.E., Wright, V.P., 1990, Carbonate Sedimentology: Oxford, Blackwells, 482p.

Tucker, M.E., 2001, Sedimentary petrology: an introduction to the origin of sedimentary rocks: London, Blackwell, 260 p.

Vaziri, S.H., 2001, The Triassic Nakhlak Group, an

exotic succession in Central Iran, in Akinci, Ö.T., Görmüş, M., Kuşçu, M., Karagüzel, R., Bozcu, M., (Eds.), Proceedings of the 4th International Symposium on Eastern Mediterranean Geology, Isparta, Turkey, 53–68.

Vaziri, S.H., Fürsich, F.T., 2007, Middle to Upper Triassic deep-water trace fossils from the Ashin Formation, Nakhlak Area, Central Iran: Journal of Sciences, Islamic Republic of Iran, 18, 263–268.

Wilson, J.L., 1975, Carbonate facies in geologic history: Berlin, Springer, 471p.

Weimer, P., Slatt, R.M., 2004, Petroleum systems of deepwater settings: Tulsa, Oklahoma, Society of Exploration Geophysicists, 470p.

Zanchi, A., Zanchetta, S., Garzanti, E., Balini, M., Berra, F., Mattei, M., Muttoni, G., 2009, The Cimmerian evolution of the Nakhlak–Anarak area, Central Iran, and its bearing for the reconstruction of the history of the Eurasian margin: Geological Society, Special Publications, 312(1),261-286. https://doi.org/10.1144/SP312.13

Zhang, C., Li, X., Mattern, F., Mao, G., Zeng, Q., Xu, W., 2015, Deposystem architectures and lithofacies of a submarine fan-dominated deep sea succession in an orogen: A case study from the Upper Triassic Langjiexue Group of southern Tibet: Journal of Asian Earth Sciences, 111- 222. https://doi.org/10.1016/j.jseaes.2015.07.013